NUMERICAL INVESTIGATION OF STATISTICAL TURBULENCE EFFECTS ON BEAM PROPAGATION THROUGH 2-D SHEAR MIXING LAYER

THESIS

James C. Bowers, Captain, USAF

AFIT/GAP/ENP/10-M03

DEPARTMENT OF THE AIR FORCE
AIR UNIVERSITY

AIR FORCE INSTITUTE OF TECHNOLOGY

Wright-Patterson Air Force Base, Ohio

NUMERICAL INVESTIGATION OF STATISTICAL TURBULENCE EFFECTS

ON BEAM PROPAGATION THROUGH 2-D SHEAR MIXING LAYER

THESIS

Presented to the Faculty

Department of Engineering Physics

Graduate School of Engineering and Management

Air Force Institute of Technology

Air University

Air Education and Training Command

in Partial Fulfillment of the Requirements for the

Degree of Master of Science in Applied Physics

James C. Bowers, B.S.

Captain, USAF

March 2010

AFIT/GAP/ENP/10-M03

NUMERICAL INVESTIGATION OF STATISTICAL TURBULENCE EFFECTS

ON BEAM PROPAGATION THROUGH 2-D SHEAR MIXING LAYER

James C. Bowers, B.S.
Captain, USAF

Approved:

_____   _____
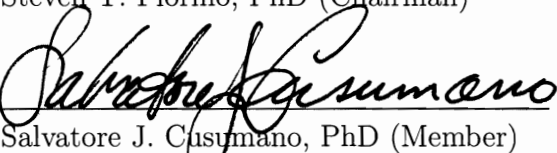Steven T. Fiorino, PhD (Chairman)   10 MAR 10
                                                    Date

_____   _____
Salvatore J. Cusumano, PhD (Member)   16 Mar 10
                                                    Date

_____   _____
Maj Andrew J. Lofthouse, PhD (Member)   16 Mar 10
                                                    Date

AFIT/GAP/ENP/10-M03

Abstract

A methodology is developed for determining the validity of making a statistical turbulent approach using Kolmogorov theory to an aero-optical turbulent flow. Kolmogorov theory provides a stochastic method that has a greatly simplified and robust method for calculating atmospheric turbulence effects on optical beam propagation, which could simplify similar approaches to chaotic aero-optical flows. A 2-D laminar Navier-Stokes CFD Solver (AVUS) is run over a splitter plate type geometry to create an aero-optical like shear mixing layer turbulence field. A Matlab algorithm is developed to import the flow data and calculates the structure functions, structure constant, and Fried Parameter (r_o) and compares them to expected Kolmogorov distributions assuming an $r^{2/3}$ power law. The range of C_n^2's developed from the structure functions are not constant with separation distance, and ranged between 10^{-12}-10^{-10}. There is a consistent range of data overlap within the C_n^2's derived from various methods for separation distances within the range 0.01m-0.02m. Within this range r_o is found to be approximately 0.05m which is a reasonable value. This particular 2-D shear mixing layer was found to be non-Kolmogorov, but further grid refinement and data sampling may provide a more Kolmogorov like distribution.

Acknowledgements

I would like to thank my faculty advisor, Dr. Steven Fiorino, for his vision, support, and enthusiasm through the completion of this research effort. Without his constant feedback, encouragement, and guidance I would still be struggling to compile and document this research. I would also like to thank the AFRL Air Vehicles Directorate Computational Sciences branch for their support in troubleshooting my CFD effort. From that group I would like to individually recognize Dr. Miguel Visbal, Dr. Matt Grismer, and Dr. Greg Brooks. Dr. Visbal was instrumental in helping me refine my grid and flow profile to produce my investigation flow field. Dr. Brooks and Dr. Grismer helped me by getting me current versions of AVUS and the necessary utility codes with the instructions on how to compile them to perform by CFD analysis. I would also like to thank the AFIT Linux administrators, primarily Dave Doak, for helping troubleshoot the parallel processing and running of the computer resources necessary to complete this investigation.

There were also some folks outside the technical aspects of this research I would like to thank. First and foremost my wife for her ceaseless support and encouragement through this endeavor. I would also like to thank my parents who have always encouraged me and believed in my potential even when I was unsure of it.

James C. Bowers

Table of Contents

List of Figures

List of Tables

List of Symbols

Symbol   Page

List of Abbreviations

NUMERICAL INVESTIGATION OF STATISTICAL TURBULENCE EFFECTS

ON BEAM PROPAGATION THROUGH 2-D SHEAR MIXING LAYER

I. Introduction

1.1 Research Overview

The advent of laser technology was described as a solution without a problem. The Air Force has made significant investments into research of new applications for laser technologies in meeting its day to day mission requirements. Researchers are investigating ways to use lasers for air and space communication, asset defense, and airborne high power directed energy effects. The critical aspect in using lasers in this manner is that they involve propagating the beam through the atmosphere, which is not necessarily the most accommodating medium. The atmosphere has many deleterious effects on laser beam propagation. These deletrious effects arise from the spectral wavelength of the source and changes in the index of refraction from density changes in the medium. They are directly attributed to three physical phenomenon: absorption, scattering, and atmospheric turbulence. These effects prevent the laser from putting the entirety of its energy or radiant intensity on a target or cause the beam to be directed away from the target, which greatly reduces the ability to precisely distribute and introduce the effects desired. By understanding how these mechanisms affect propagation, these beam quality issues can be better anticipated and mitigated.

While absorption and scattering are important phenomenon, the focus of this research is turbulence. Turbulence is instability in motion of fluid, or the atmosphere.

1

Turbulence arises from injection of energy into the fluid causing the motion to become unstable. This source of this energy injection is usually introduced thermally from temperature gradients with height in the atmosphere or aerodynamic friction along the ground, ocean, the skin of an aircraft, or any other surface. Turbulence is often represented physically by whorl-like structures called eddies. These eddies come in many shapes and sizes which leads to a need to describe these eddies with respect to a scale. In the instances above, atmospheric eddies within the inertial sub range can range from 200 meters to 0.002 meters compared to the aerodynamic eddies, which can be described as microscopic as they are on the order of 2 millimeters and smaller.

Being able to model and predict turbulence is quite challenging because of its large range of length and time scales. The injection of kinetic energy to produce the larger eddies begins to fade into to smaller and smaller eddies. Because of the small size scale of the initial eddies and the time scale over which the energy is injected into the fluid makes it difficult to describe the behavior numerically real-time. Computing turbulence real-time would require a very fine resolution evolution in time and space, and would only be accurate for a very small period of time. This would require a large number of computational resources and time to compute. There are other numerical methods, such as Large Eddy Simulation, that model turbulence behavior as chaotic or random while the fluid flow evolves as solved using the Navier-Stokes equations. Therefore, statistical or stochastic methods such as Kolmogorov's method were derived for the purpose of simulating beam propagation effects.

The heart of this research is investigating the effects the resultant turbulence fields from these different modeling approaches has on propagating a laser through the atmosphere. Does micro-scale aerodynamic turbulence described chaotically produce turbulence fields that affect simulated laser beam propagation in a quantifiably different way than atmospheric turbulence modeled statistically? By classifying which

model has the more dominant effect on the beam could change the approach engineers take to mitigate atmospheric turbulence effects on propagation. It may also cause researchers to reevaluate approaches to analyzing the modeling descriptions of atmospheric turbulence.

1.2 Brief Background

1.2.1 Atmospheric Effects on Lasers.

Laser is the short hand form for Light Amplification through Stimulated Emission of Radiation. A laser works by taking an input electromagnetic radiation source and amplifies it by producing additional electromagnetic radiation produced by the quantum mechanical means of stimulated emission through a receptive gain medium. The major aspect of this process is that it leads to an increased irradiance of electromagnetic radiation which carries increased spectral power in a specific wavelength, frequency, and polarization. Notice the word light has not been used in the above description. This is to keep the discussion relevant to any radiation that falls within the electromagnetic spectrum. The nature of this electromagnetic radiation in regards to light is rather complex with regard to it being made up of corpuscular components referred to as photons or as waves. Regardless of which form actually describes light it is important to understand that this amplified radiation is susceptible to phenomenon that can alter the amount of radiation that arrives to its final destination or where that final destination is.

Diffraction is the redirection of the wave front or ray due to a change in the optical properties of the medium through which the wave or ray is traveling. The optical property of the medium is often referred to as the index of refraction. The refractive index is typically dependent on wavelength of the incident radiation and the density of the medium. Therefore, slight density changes in, for example, the atmosphere

due to turbulence, affect the direction and intensity of the beam as it traverses the medium.

Atmospheric extinction is the reduction of the incident radiation through the atmosphere due to absorption and scattering effects. In the same manner that the laser beam is created by the quantum mechanical means of stimulated emission, it is also susceptible to giving up its energy to molecules along the path that would be receptive to the quantum mechanism of absorption. The energy can also be lost through absorption by inducing motion of the molecule through rotation or vibration. This is a major consideration due to the number of different molecules that constitute air, as well as water and the numerous available aerosols in the atmosphere. The nature of these losses is primarily wavelength driven and is usually mitigated in the operational design wavelength bandwidth of the laser. [11]

Absorption also contributes to another deleterious effect on beam propagation in the form of thermal blooming. As the air and other atmospheric constituents absorb the incident radiation, that energy often takes the form of heat. Heat produces thermal gradients in the air which results in density changes in the medium. As stated above, these density changes result in local changes in the index of refraction, which can shift the direction of the beam. [11]

Scattering is an extinction mechanism in that it removes energy from the laser beam by redirecting the radiation through elastic collisions with present particles in directions not in the direction of propagation. While the incident radiation is not necessarily lost or destroyed in the action, the beam has now lost some of its constitutional integrity, reducing the amount of radiation on target. This mechanism is again primarily wavelength dependent and can be compensated by design considerations for the operational window of the laser. [11]

These mechanisms represent a few of the design challenges facing engineers in

4

the incorporation of laser systems for military application in air and space. The above effects are losses in energy due to atmospheric extinction which are mostly wavelength dependent. However, diffraction due to refractive index changes is driven by density changes. Turbulence must be carefully considered in system design, as turbulence introduces varying local density changes, providing a dynamic refractive index change. By better understanding sources of turbulence and how to describe them are crucial when trying to address laser integration into Air Force systems.

1.2.2 Turbulence.

As mentioned earlier, turbulence is instability in fluid flow, which causes localized variances in fluid speed and density. The source of these instabilities is the introduction of additional kinetic energy into the flow. Atmospheric turbulence can be characterized by three means: mechanical, thermal, and inertial. Mechanical turbulence is the result of variance in the wind speed at various layers referred to as shear. The changes in shear can be attributed to surface drag, wake flow, or free stream shear. Surface drag creates variations due to slower wind speeds at the surface, due to friction, than speeds higher aloft. Wake flow is effect of surface roughness or protuberances from the surfaces, such as trees or buildings, which cause wind speed variations as the fluid must move around these obstacles. Free stream shear is wind speed variations that occur naturally away from any solid surface. Thermal turbulence is result of changes in temperature, usually from radiative heating or cooling, that cause air to rise or sink buoyantly. Inertial turbulence is the product of the loss of kinetic energy of eddies, which leads to a dissipation of eddies into smaller and smaller eddies. [20]

In light of these mechanisms for creating or affecting existing turbulent sources, turbulence is highly dynamic in nature, and hard to predict. In this regard, the

constantly changing size and time scales for how the dissipation occurs is hard to model and predict as these changes are often random or non-linear, and require very small scale spatial resolution to capture the physics or become very inaccurate for longer time scales. This inability to accurately capture turbulent flow behavior led to two very different approaches in modeling turbulence: chaotic, allowing the random behavior to evolve in the flow, or statistical, developing a parameterized description of the turbulence with regard to temperature range and average velocities. [20]

The current problem in approaching turbulence effects on laser beam propagation is that there are two ranges or regions of turbulent flows that have contrasting viewpoints, scales, and assumptions made that has divided the research community in this field. The first viewpoint is that atmospheric turbulence is the dominant factor. The strength of this approach is that because of the ranges and somewhat predictable nature of the atmosphere allows certain assumptions to be made which allows for a more simplified or standardized approach to addressing turbulent effects on beam propagation. The weakness is that it ignores small scale turbulent features that may be present in, for example, an airborne system that has boundary layer turbulence over an aperture. The second viewpoint is that these aero-optical features cannot be ignored. The strength of this approach is that it allows for a more complete account for turbulent effects on beam propagation. The problem though is that the smaller scale and unpredictable nature of these aero-optical eddies make it difficult to make the same assumptions that a statistical viewpoint uses.

The presiding theory for the statistical representation of the atmosphere is the Kolmogorov Theory of 1941. Kolmogorov theory provides a way to parameterize the eddy size scale, velocity and temperature profiles, to provide structure constants that describe the nature of the turbulence within that range. Using these structure terms, optical parameters can be developed and used to predict the behavior of a wave front

to propagate through the turbulence. This theory is very useful; however it is only applicable to modeling turbulence effects on optical performance within the inertial sub-range of turbulence. [2]

A lot of the analytical work for investigating aero-optical turbulence is performed using numerical models. Modeling numerical fluid flow can be accomplished using the Navier-Stokes equations. Numerical modeling of fluid dynamics using the Navier-Stokes equations has become very robust, and there are many commercially available flow solvers that allow these flow physics to be calculated. As understanding of turbulence behavior has evolved, mathematical models that predict the unsteady nature of turbulence have been incorporated with these Navier-Stokes solvers to provide a characteristic representation of the random nature of turbulence. These computational flow simulations provide some opportunities to investigate the fluid dynamics around an airborne system. As previously stated though, these simulations can be very time consuming to generate as they require small temporal and spatial scales, and large amounts of processing to generate. Even then these simulations may only be qualitatively representative rather than quantitatively useful. Therefore, these simulations are representations of representative flow condition or used in diagnostic of what the flow may be like, and not neccesarily useful for a rigorous or accurate accessment of turbulent effects.

However, if there is little difference between a characteristic aero-optical flowfield and its statistical representation then there would be an opportunity to reconcile these two approaches and simplify the way engineers design and compensate for both atmospheric and aero-optical turbulence. This is fundamental motivation for this research.

1.3 Investigative Setup and Scope

In order to create the basis for this comparison of turbulence effects, a fluid flow similar to an aero-optic flow will be generated using Laminar Navier-Stokes approaches that are available in Computational Fluid Dynamics (CFD) software. A two-dimensional (2-D) splitter plate type geometry to generate a laminar shear layer as representative turbulent field for analysis. The output from the fluid model will then be accessed using stochastic methodologies to determine if this characteristic aero-optical turbulent flow field has Kolmogorov like qualities.

1.4 Outline of Thesis

The remainder of this document is divided among 4 chapters following this introduction. Chapter two is an in depth discussion of all relevant theory to the investigation, as well as a look at previous or current research into this particular approach or topic. Chapter three will state with more detail the research approach, providing a more detailed technical description of software used, and specific parameters being considered for matters of comparison. Chapter four will present the results of the conducted research and will provide a thorough analysis of the collected data with regards to the nature of the research. Chapter five will conclude this thesis. It will provide a short summary of results, and provide insights with regards to future research along this topic.

II. Background and Theory

This chapter presents the reader with a review of any pertinent background, theory, and research previously conducted in this field of study. Chapter two begins with a discussion of atmospheric effects on laser beam propagation. A more in depth discussion of turbulence is then provided. After establishing a background on turbulence, a review of Kolmogorov's Theory is provided as means to discuss a statistical means for analyzing turbulence effects on beam propagation. A summary is then provided presenting researched examples of where Kolmogorov's theory is not capable of capturing the effects of turbulence on beam propagation. There is then a discussion of fluid mechanical studies on turbulence effects for aero-optical applications. The chapter finishes with a quick discussion of Computational Fluid Dynamics (CFD) simulation tools to be used in this study.

2.1 Atmospheric Effects on Lasers

Light is susceptible to many forms of alteration due to diffraction and attenuation. The atmosphere can produce the means to introduce these influences in the form of atmospheric extinction due to scatterring and absorption, and atmospheric turbulence. These mechanisms represent a few of the design challenges facing engineers in the incorporation of laser systems for military application in air and space. Atmospheric extinction effects are mostly wavelength dependent. Atmospheric turbulence introduces density changes in the medium leading to diffraction from refractive index changes. An example of how optical density affects wave propagation can be seen in Figures 1 and 2. As optical density increases the transmitted wavefronts rotate away from the incident axis as seen in Figure 1. With the dynamic nature of turbulence, the optical density gradient varies with time, which creates transmission fluctuations

as seen in Figure 2. Turbulence influence on beam performance is difficult to mitigate because of its inherently unpredictable nature. By better understanding sources of turbulence and how to describe them are crucial when trying to address laser system integration for Air Force applications. [11]
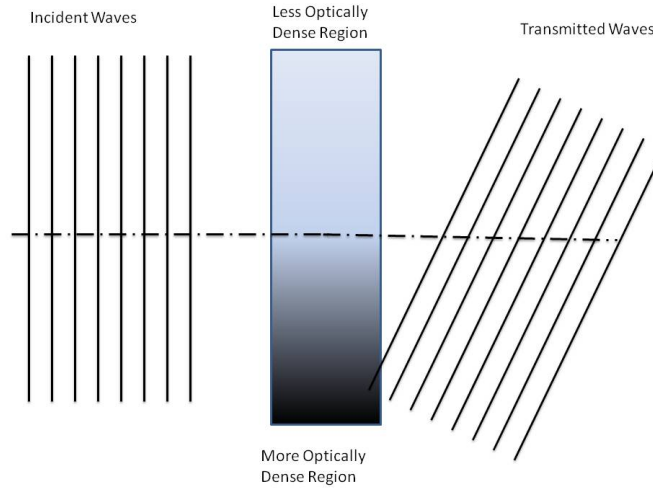
Figure 1. Illustration of Non-Dynamic Refractive Medium on Propagation
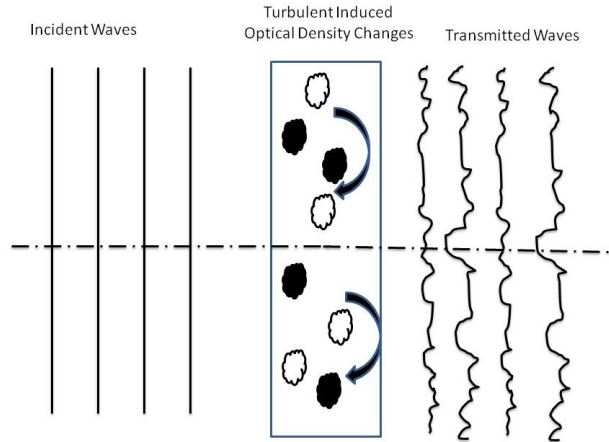
Figure 2. Illustration of Time Varying Refractive Medium on Propagation

2.2 Turbulence

In order to analyze the effects of turbulence on beam propagation, it is important to understand what turbulence is, where it comes from, and some representative characteristics that represent it. Turbulence derives from instabilities in fluid flow. It is characterized by irregularity, or non-linear behavior. This randomness results in the development of rotational structure called eddies, swirling in all directions. These whirling eddies make the turbulent flow diffusive, causing rapid mixing which increases the rates of transfer in momentum, heat, and mass. Turbulence is also dissipative in that viscous forces increase the energy of the fluid, which causes kinetic energy of the turbulence to decrease in order to maintain energy conservation. If there is no further injection of kinetic energy into the flow, then turbulence will decay rapidly.[17]

It is now important to understand what causes turbulence. The source of atmospheric turbulence is the introduction of additional kinetic energy into the flow. Turbulence can be introduced by three means: mechanical, thermal, and inertial. Mechanical turbulence is the result of variance in the flow speed at various layers referred to as shear. The changes in shear can be attributed to surface drag, wake flow, or free stream shear. In atmospheric turbulence, surface drag creates variations due to slower wind speeds at the surface, due to friction, than speeds higher aloft. Wake flow is effect of surface roughness or protuberances from the surfaces, which cause wind speed variations as the fluid must move around these obstacles. Free stream shear is just level wind speed variations that occur naturally away from any solid surface. Thermal turbulence is result of changes in temperature, usually from radiative heating or cooling in the atmosphere, that cause air to rise or sink buoyantly. Inertial turbulence is the product of the loss of kinetic energy of eddies, which leads to a dissipation of eddies into smaller and smaller eddies as describe above.[20]

These characteristic make it easy to see that turbulence by nature is very non-linear. This makes it very difficult if not impossible to describe turbulence spatially or temporally with any precision. This inability to accurately capture turbulent flow behavior led to two very different approaches in modeling turbulence: a chaotic aproach which allows the random flow behavior to evolve using some numerical microphysics model, or statistically developing a parameterized description of the turbulence with regard to temperature range, eddy scales, and average velocities.

Turbulence was first systematically investigated by Osborne Reynolds in 1883. His major contribution to the field was the introduction of a nondimensional means for characterizing turbulence.

$$Re = \frac{ul}{\upsilon} = \frac{\text{Inertial Transport}}{\text{Viscous Transport}} \tag{1}$$

The Reynolds Number (Re) as seen in Equation 1 is determined by the flow speed (u), scale length (l), and viscosity (υ). The Reynolds number can provide a classification of the strength of turbulence. Lower numbers represent a laminar turbulent flow which is more smooth and less irregular. Higher numbers represent strong turbulence characterized by random and irregular flow.[4]

As the Reynolds number increases, the separation of length and time scales increases as well. These increases introduce more chaotic flow conditions with them that are hard to define mathematically. In order to begin a statistical assessment of turbulence, a dimensional analysis is necessary. This involves the development of scales for the size of the turbulent eddies. The eddies which constitute turbulence represent a spectrum as seen in Figure 3. This spectrum can be classified by three regions: The Production Subrange, the Inertial Subrange, and the Dissipation Subrange. The production subrange is where kinetic energy is introduced in the flow to create turbulent eddies. Turbulence in this region is very anisotropic and not gov-

erned by any general description. Eventually that turbulent kinetic energy starts to be lost into the internal energy of the flow by molecular viscosity. When those viscous forces dominate the kinetic energy, the flow enters the dissipation subrange. This region represents the smallest eddy structures. In between these regions is the inertial subrange. This subrange is where the energy lost to heat is very small compared to the transfer of energy into the turbulent scales.[20; 8]
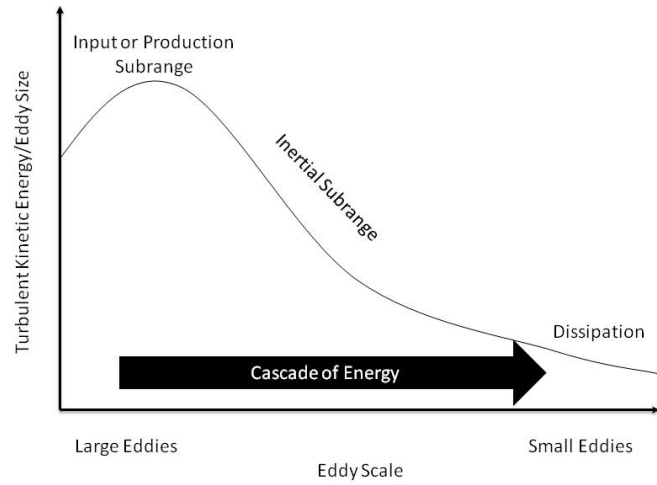
Figure 3. Cascade of Turbulent Kinetic Energy

Now that these subregions for the spectrum have been introduced, it is important to know where sizing scale is derived from. Figure 4 is a representation of how scaling size originated from the cascade of eddies through the turbulence spectrum. The inertial subrange begins when there is no further injection of kinetic energy into the flow. The upper boundary (L_o) represents the size of the largest eddy present as energy injection ceases. The kinetic energy continues to dissipate from this point, however it is inviscid, energy transfer into turbulent scales is greater than energy transfer into heat. The lower bound (l_o) is the smallest size that eddies will take

13

within the inertial subrange. Below l_o the dissipation mechanism is friction due to viscosity. The lower boundary is usually the transition from laminar to turbulent flow. When the eddy size is between these bounds the turbulence is considered to be in the inertial subrange. The utility is that theory suggests that by establishing these boundary scales, the inertial subrange is homogenous and isotropic which is useful in developing a statistical representation for the flow conditions that may affect beam propagation. [8]
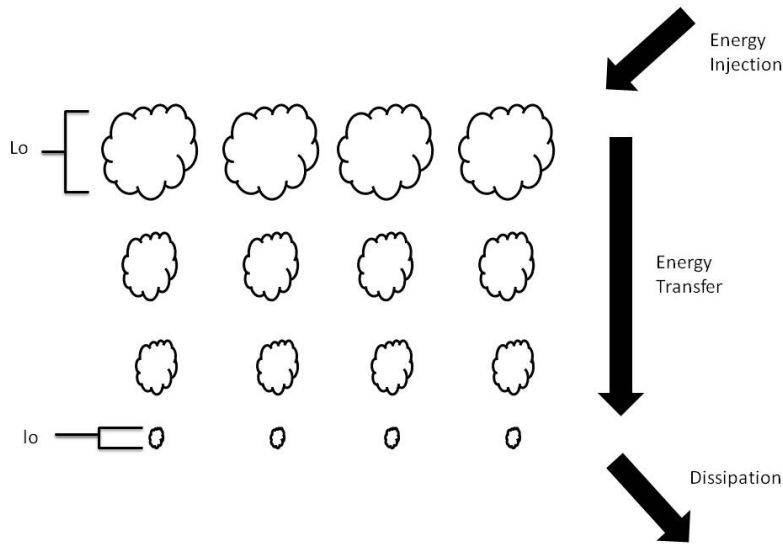
Figure 4. Depiction of Eddy Dissipation and Scales

2.3   Statistical Representation of Turbulence

2.3.1   Defining Optical Parameters.

Before discussing Kolmogorov Theory, it is important to understand some of the optical parameters that are used to determine the statistical representations of a turbulent field and how they are derived.

2.3.1.1 Index of Refraction.

The refractive index (n) of a medium is the degree to which a wavefront will be redirected as it propagates as presented and illustrated previously. For free space or a vacuum there is no refraction and the refractive index is set to unity. Stable air has a refractive index that is very close to unity. However turbulence and atmospheric air constituents provide variations in density and wavelength dependent affects that can create slight deviations from that of stable air, which effects propagation. There are several empirically derived methods for finding the local index of refraction at a point in the atmosphere depending on beam wavelength, and local pressure, temperature, and density. The first is the Edlen formula as seen in Equation 2,

$$n(x, y, z, t) = 1 + (10^{-8})(8342.12 + \frac{2406030}{130 - \frac{1}{\lambda^2}} + \frac{15997}{38.9 - \frac{1}{\lambda^2}})(\frac{\rho(x, y, z, t)}{\rho_o}) \qquad (2)$$

which is dependent on the wavelength (λ in μm) the spatial value of density $(\rho(x, y, z, t))$ and the reference or standard density (ρ_o). The second is the Gladstone-Dale Method as seen Equation 3,

$$n(x, y, z, t) = 1 + K_{GD}\rho(x, y, z, t) \qquad (3)$$

which uses a constant (K_{GD}) which has been derived empirically and the spatial value of density $(\rho(x, y, z, t))$. The Gladstone-Dale for a 1 micron beam is approximately $2.25 \times 10^{-4} \frac{kg}{m^3}$. [21; 12]

2.3.1.2 Phase, Optical Path Length, and Optical Path Difference.

Turbulence distorts the phase front of a plane wave. There are two mathematical means that can be used to describe the amount of phase (ϕ) alteration that occurs due to turbulent abberations. The first is the Optical Path Length (OPL). The OPL

through a medium and be approximated using Equation 4,

$$OPL(x, y, z, t) \approx \int^{s} n(x, y, z, t) \, ds \tag{4}$$

where s represents the propagation path length and $n(x, y, z, t)$ represents the spatial refractive index along that path. The wave's phase (ϕ) can be found from the OPL using Equation 5,

$$\phi = k_o OPL(x, y, z, t) \tag{5}$$

where k_o is the wavenumber ($k_o = \frac{2\pi}{\lambda}$). The second means of mathematical describing the wavefront distortion is the Optical Path Distance (OPD) which is the difference in the OPL relative to the mean over an apperture as seen below in Equation 6,

$$OPD(x, y, z, t) = OPL(x, y, z, t) - \overline{OPL(s)} \tag{6}$$

where $\overline{OPL(s)}$ represents the average of the OPL's along a simulated plane perpendicular to the beam path. [19]

2.3.2 Kolmogorov Theory.

At the forefront of this statistical representation of Turbulence is the Kolmogorov Theory of 1941. Kolmogorov theory provides a way to parameterize the eddy size scale, velocity and temperature profiles, to provide structure constants that describe the nature of the turbulence within that range. The boundary for this characterization is dependent on the scale size of the turbulent eddies as described above. Kolmogorov theory of 1941 provided two definitions from which to make the determination that a turbulence distribution could be called homogeneous and isotropic. These definitions define the boundaries of the inertial subrange. Kolmogorov also contributed two hypothesis on similarity which provides a way to develop parameters for analysis

assuming a homogeneous, isotropic distribution.[9]

The first similarity hypothesis says that at a significantly high Reynolds number an isotropic turbulence distribution can be defined by the values of $\bar{\varepsilon}$, the average energy dissipation rate, and ν, the viscosity. The average energy dissipation rate ($\bar{\varepsilon}$)is defined by the mean fluid velocity ($\bar{u}$) and the outer scale length (L_o) by the following relationship in Equation 7:

$$\bar{\varepsilon} \sim \frac{\bar{u}^3}{L_o} \tag{7}$$

The second similarity hypothesis states that flows with sufficiently high Reynold's Numbers, within the inertial subrange where the dominant turbulence process is inertial transfer in to turbulent scales rather than in to viscous creation of heat, then the distribution is dependent only on the energy dissipation rate ($\bar{\varepsilon}$). [10]

A representative example of this can be found in Figure 5. The Energy Spectrum should look familiar. It is much like that presented in Figure 3. The major differences between these representation of scales as Figure 5 is semilog, and that the independent axis is wavenumber as opposed to eddy size. Using these similiarity hypothesis Kolmogorov was able to build an expression for the kinetic energy spectral density as presented in Equation 8

$$E(k_o) = K\bar{\varepsilon}^{\frac{2}{3}}k_o^{\frac{-5}{3}} \tag{8}$$

The exponents in Equation 8 are found using dimesional analysis. The K in Equation 8 represents a constant. This constant is what makes the curve fit as seen in Figure 5 to the spectral density function within the inertial subrange. It is this approach that provides a method for the development of structure functions and the associated fit parameters such as C_n^2. [14]
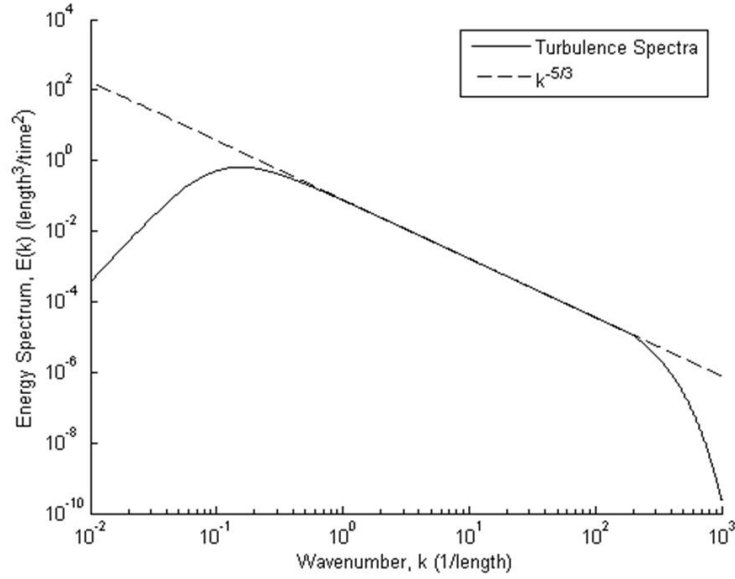
Figure 5. Turbulent Energy Spectrum and Fit Example. [14]

2.3.2.1 Structure Functions.

A structure function is a statistical discription of the average of the differences squared of two parameters separated by a distance, r. Equation 9, which is an autocorrelation function commonly used in turbulence studies, provides a representative view of this concept where χ represents some parameter (velocity, phase, etc) and r represents the distance between the reference and the point of interest.

$$D_\chi(r) = \overline{(\chi(0) - \chi(r))^2}$$ (9)

Figure 6 is a representation of the velocity structure function created in the same manner. By making the assumption that the flow is isotropic and homogeneous there will be no difference in this function no matter the reference orientation is made. In Figure 6 it is important to note behavior at the extremes of the position scale. As the scale size becomes small there is very little variation in the velocity field so it goes to

18

zero as the separation gets smaller. As the separation get larger the function tends to become constant as the differences in the spatial parameter start to average out to a constant value. Using an $r^{2/3}$ fit relationship there is a region where the fit coincides well with the structure function. This region represents the inertial subrange. The structure function can be found to fit within this region by the following relationship.

$$D_v(r) \cong C_v^2 r^{\frac{2}{3}} \tag{10}$$

In Equation 10 two important things are presented. The first is the $r^{2/3}$ relationship. The second is the fit constant C_v^2, which is how the curve fit is made. This Structure Constant can give some indication of how relatively weak or strong the fluctuations are.
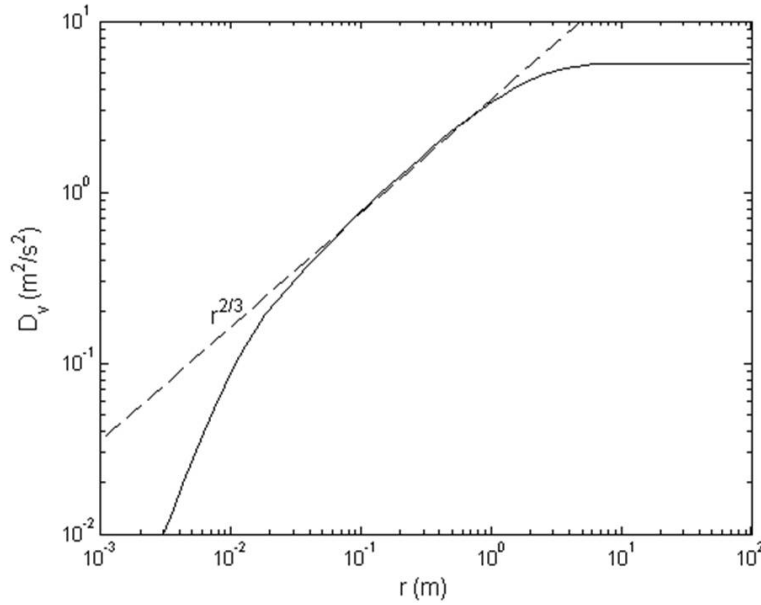
Figure 6. Velocity Structure Function and Fit Example. [14]

This can be used to create a structure function, $Dn(r)$, for the index of refraction

19

as seen below in Equation 11.

$$D_n(r) = \begin{cases} C_n^2 l_o^{\frac{-4}{3}} r^2, & 0 \le r \ll l_o \\ C_n^2 r^{\frac{2}{3}}, & l_o \ll r \ll L_o \end{cases} \qquad (11)$$

The index of refraction structure constant (C_n^2) is inferred from the variability of the index of refraction shown in Equation 11. C_n^2 is typically in the range of 10-12 for cases of strong turbulence to 10-17 in weak cases. For atmospheric representations, C_n^2 is typically derived from C_T^2 which is constructed from thermal gradient data collected in the atmosphere by the relationship seen in Equation 12. [2]

$$C_n^2 = C_T^2 (79 \times 10^{-6} (\frac{P(mbars)}{T(K)}))^2 \qquad (12)$$

2.3.2.2 Fried Parameter.

In trying to optimize resolving power of an optical system, D. L. Fried developed a normalized signal-to-noise ratio ($\psi(\frac{D}{r_o})$) as a function of the aperture diameter (D) and a length scale (r_o) which is often defined as the Fried Coherence Length or Fried Parameter. [5] Figure 7 is a plot of this function. The Fried Parameter is found at the intersection of the two assymptotic limits at $\frac{D}{r_o} = 1$. The Fried Parameter can be found from the structure function of phase and amplitude for normalizing the Fried signal-to-noise ratio by the relationship provide below in Equation 13.

$$D_\phi(r) + D_{ln(A)}(r) = 6.88(\frac{r}{r_o})^{\frac{5}{3}} \qquad (13)$$

The Fried Parameter is a way to describe the point of diminishing returns for improving signal quality by increasing the aperture diameter to create a diffraction limited beam.
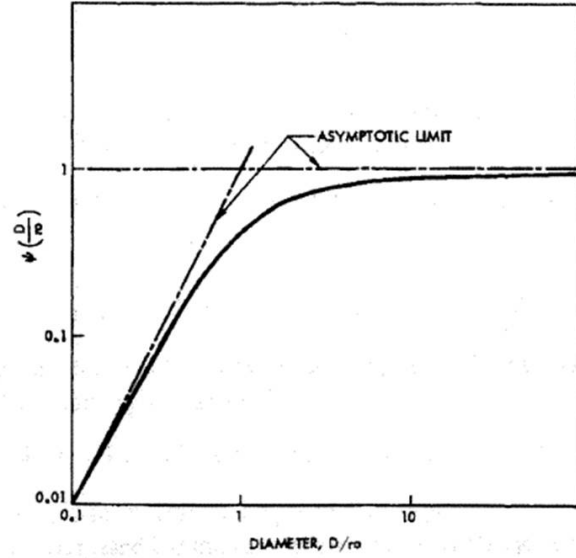
Figure 7. Fried's Normalized Signal-to-Noise ratio. [5]

The Fried Parameter can be found with a given C_n^2 using the expression below in Equation 14 for a plane wave,

$$r_o = [(\frac{2.905}{6.88})(\frac{2\pi}{\lambda})^2 \int_0^R C_n^2(s)\,ds]^{-3/5} \qquad (14)$$

where R is the path length or range. If $C_n^2(s)$ does not vary much over that range then it is possible to simplify that expression to Equation 15 for a plane wave. [11]

$$r_o = 0.185 \frac{\lambda^{\frac{6}{5}}}{R^{\frac{3}{5}} C_n^{2\,\frac{3}{5}}} \qquad (15)$$

2.4   Deviations from Kolmogorov

By now understanding the origins of the stochastic representation of turbulence, it is important to note that there are several problems when trying to capture the effects of atmospheric turbulence on beam propagation using Kolmogorov representation. The first is the fact that it is only viable in the inertial subrange of eddy structure.

21

The second is that it assumes a homogeneous, isotropic distribution of turbulence. However by its nature turbulence is anything but homogeneous and isotropic. Localized turbulent disruptions and non-uniform distributions lead to anisotropy. Turbulence structures are not only circular, but have helicity to them which can form localized patches of anisotropy.

Golbraikh et al found that using Lidar measurements to compare vertical turbulence profiles, that Kolmogorov theory cannot accurately describe turbulence effects on optical beam propagation. [6] Toselli et al summarized recent experimental results that did not agree with analytical techniques utilizing Kolmogorov theory for atmospheric turbulence. Mechanisms for these deviation stem from density anisotropy, helicity of turbulence, and atmospheric boundary layer stability. [18] Shugaev et al found that the Kolmogorov theory does not accurately provide the correct structure definitions for flow fields that include strong disturbances and non-uniformity of the medium. The results also indicate that in order to capture turbulent flow accurately, it is necessary to have a large number of data points in order to get the appropriate structure resolution. [13] Sirazetdinov et al compared the results from an experiment collecting laser beam propagation data through a turbulent engine flow field with that of an analytical model using Fresnel transformation with randomly inhomogeneous phase screens. [15] They found that there is some improved accuracy between experiment and computations, which suggest that accounting for a chaotic turbulent flow field may be needed to accurately capture turbulence effects on beam propagation.

2.5   Fluid Studies and Aero-Optics

There have been several studies to determine the behavior of turbulence for applications in aero-optics. Siegenthaler et al provided a compilation of the prevailing statistical methods and parameters with the assumptions needed to apply them and

compared them to the effects of an aero-optical flow field. [14] They conclude that making stochastic assumptions are not viable for describing aero-optical flows because Stochastic methods are primarily driven by thermal gradients while aero-optical turbulence is driven primarily by flow gradients in the shear layer. They do say that these statistically derived parameters could be viable on a case by case basis for detailed scenarios. Zubair et al provides two important perspectives to this research topic. [22] The first is that the large scales of turbulent structure provide more dominant effect on aero-optical performance. The second is that a Large Eddy Simulation(LES) turbulence model provides enough resolution to evaluate aero-optical performance. High Reynolds number flow fields are dominated by smaller scale turbulent eddies. While large scale eddies have more deleterious effects on beam propagation, small eddies contribute to beam degradation as well, but are slightly more difficult to measure and predict. Catrakis et al took the approach of combining CFD research with an experimental method to observe fluid turbulence. [3] The work compared experimental results with computational simulations to observe aero-optical effects. The major finding was that the turbulence behavior is non-monotonic, which means that there are non-linear effects in turbulence that may not be able to be resolved purely statistically. Aguirre et al found that at higher Reynolds numbers, the number of small-scale features increases which creates the inability to compare the propagation effects from large scale with regard to small scale structures. Small scales are consistent with similarity theory for statistical means of representation. [1] However there still exists a large anisotropy of the density which must be compensated for when computing wave front propagation.

Visbal researched effects on optical propagation through the shear layer of turbulence for various airspeeds using two dimensional high-order numerical fluid methods. [19] The conclusions found that transmission aberrations compared using Optical

Path Difference can manifest due to primarily compressibility effects, despite very different density field distributions. This suggests that there is no one-to-one correspondence between integrated optical aberration and the flow structure, meaning that there are several mechanisms contributing to adverse propagation effects through turbulence.

These studies provide some interesting insight into the shortcomings of Kolmogorov theory and the difference in approaches between atmospheric and aero-optics turbulence communities. Kolmogorov is useful for atmospheric turbulence in that provides a robust method for accessing the affects of the atmosphere on beam propagation despite slight deviation from the prevailing theory. Atmospheric turbulence community also uses thermal gradients in their determinations as it is the primary source for atmospheric turbulence and is data that is easily obtained from meterological instrumentation. Aero-optical turbulence consists of turbulent scales that are smaller in scale driven by flow gradients in the shear layer. These eddies are susceptible to compressibility factors creating density gradients changing the refractive index as opposed to thermal gradients. The largest scales of turbulence in aero-optics flows are the most dominant influence on beam propagation, and the ability to manage or decrease their size will have less critical effects on beam propagation. This is relevant to this research by investigating if these differences in approach are quantifiably different, and that even if they are, will the difference significantly alter what method is chosen to analyze an aero-optic flow's affect on beam propagation.

2.6 CFD Tools and Use in Aero-Optical Investigations

Modeling numerical fluid flow can be accomplished using the Navier-Stokes equations. Numerical modeling of fluid dynamics using the Navier-Stokes equations has become very robust, and there are many commercially available flow solvers that

allow these flow physics to be calculated. As understanding of turbulence behavior has evolved, mathematical models that predict the unsteady nature of turbulence have been incorporated with these Navier-Stokes solvers to provide a characteristic representation of the random nature of turbulence.

One of these is the Government developed code, the Air Vehicles Unstructured Solver (AVUS). AVUS is an unstructured, cell-centered, finite-volume, Godunov-type solver that uses least-squares gradient reconstruction and limiting for second-order spatial accuracy, and second-order, point-implicit time integration. [7; 16] The commericial equivalent of AVUS is Cobalt. Rennie et al used Cobalt to compare a 2-D compressible shear layer to a Weakly Compressible Model. [12]

III. Methodology

This chapter presents the reader with the steps taken to conduct this investigation. The primary scope of this research is to develop a methodology by which to make these assessments with a variety of scenarios. As an initial test case the flow scenario will be a 2-D laminar Navier-Stokes solver weakly compressible aero-optical like flow field. In order to create the basis for this comparison of turbulence effects, a fluid flow similar to an aero-optic flow will be generated using a laminar Navier-Stokes solver used in CFD software. A 2-D splitter plate type geometry is used to generate a laminar shear layer as representative turbulent field for analysis. Stochastic methodologies will then be used to assess this output and determine if this characteristic aero-optical turbulent flow field has Kolmogorov like qualities.

Figure 8 provides a visual representation of the workflow for this research. There are three primary phases to accomplishing this. The first is pre-processing or the preparing of inputs for processing. A geometry configuration is selected and a cartesian grid is constructed. Combining this grid with the boundary conditions and the run script the CFD process may begin which is one of the components for the second phase, Processing. Processing is the computation of the flow and calculation of the optical parameters from the flow data. The last phase is Post-Processing. Post-Processing is the required steps to examine the flowfield and assess that the data is either complete or sound, and then to analyze the statistical parameterization.

3.1 Geometry

The geometry to be used for this investigation is a 2-D splitter plate. Figure 9 is an exaggerated illustration of this geometry. A splitter plate is a thin sheet. The flow above and below are set to varied speeds. When the flow reaches the end of the
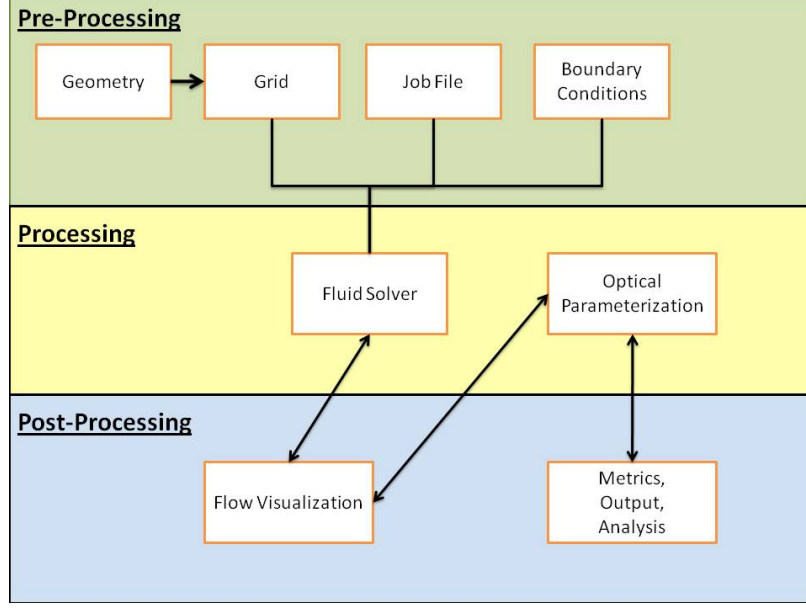
Figure 8. Work Flow Chart for the Investigation

plate the shear induced turbulence will evolve. For this case, the freestream Mach number (M_∞) above the plate is set to 0.6 ($M_{1,\infty} = 0.6$). Below the plate it is set to 0.1 ($M_{2,\infty} = 0.1$). This is consistent with making the laminar shear layer weakly compressible and is similiar to the values set in Visbal and Rennie et al. [19; 12]

3.2   Grid

A cartesian grid was created using the software package Gridgen. A structured grid was used due to the simplicity of this geometry, improved control on mesh spacing, and the fact that my statistical parameterization algoritm uses a structured grid.

Before building the grid it was necessary to make some calculations regarding the minimum grid spacing at the end of the plate so as to be able to capture the flow physics within the boundary layer. The boundary layer thickness (δ) at the end of the plate can be found by using Equation 16 for a laminar boundary layer as seen
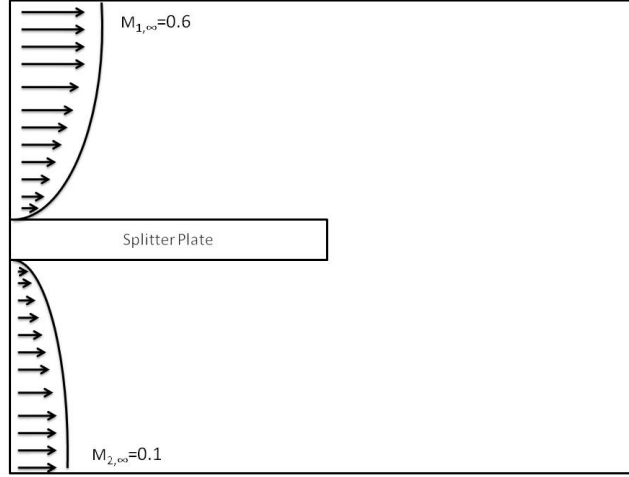
Figure 9. Work Flow Chart for the Investigation

below.

$$\delta = \frac{0.37 l_p}{Re^{\frac{1}{3}}} \tag{16}$$

For the purposes of defining δ, the Reynold's Number was set to 4000 ($Re = 4000$). This Reynold's Number was used because the flow solver is using the Laminar Navier-Stokes equantion and a Reynold's Number of 4000 is consistent with previous research for the purpose of a laminar flow analysis. In defining the geometry the splitter plate length (l_p) is set to $1m$ to better allow the flow to develop. From these parameters the boundary layer thickness is found to be, $\delta = 0.023m$. This was determined by using the top layer free stream velocity and assuming that the lower layer free stream velocity would generate a similiar boundary layer thickness as was used in previous research.

In order to include 10 grid points with in the boundary layer using a geometric growth rate of 1.2 for the node spacing a minimum grid spacing (δ') was found to be $0.00075m$. The width of the splitter plate was set to $2\delta'$ in order to the plate thin. From these calculations the grid was created. Figure 10 is a view of the whole grid.

The entire grid has a dimension of $6m \times 7m$. The grid dimensions are exagerated so as to try to eliminate interference within the area of interest from reflections and other boundary influences. The detail within the area is sufficient enough so as to capture the flow physics. Figure 11 shows the grid zoomed in to the edge of the splitter plate. This view gives an idea of the growth and mesh size based on the above definitions.
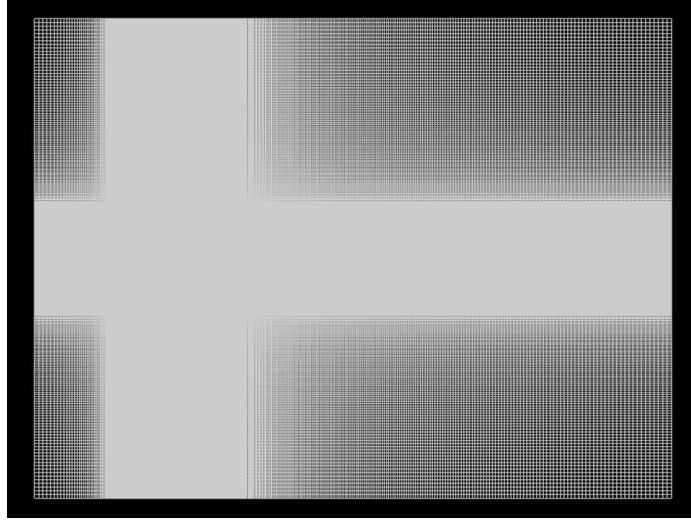
Figure 10. Grid Used for Flow Computation
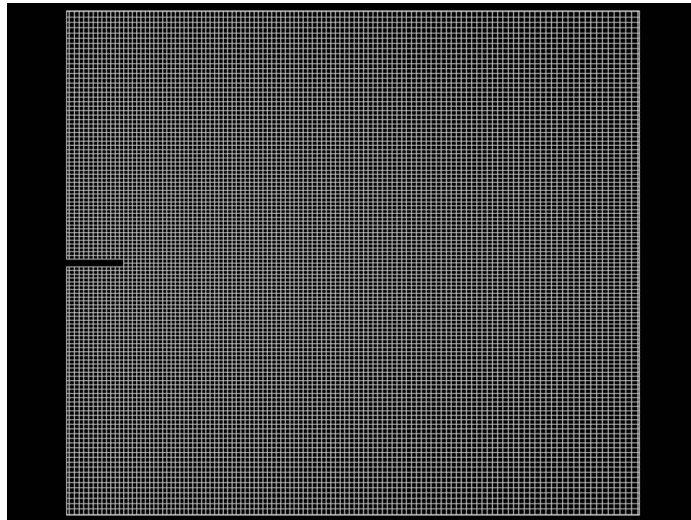
Figure 11. Zoomed in View of the Grid

3.3   Boundary Conditions

The boundary conditions tell the flow solver what conditions are to be held constant or parameterize the behavior of the flow along the geometry boundaries. The inlet regions were set to source boundaries as they will be where the flow will be introduced from. The parameters of these boundaries are built on assuming Standard Temperature and Pressure (STP) with the Mach numbers for the upper and lower surfaces set to values specified in the geometry session. The top and bottom boundaries are set to slip walls so as to bound the flow but not create another boundary layer that would be introduced if it was a solid wall. The outflow region is set to a farfield boundary as it is sufficiently downstream from the area of interest so as not to affect the flow there. The splitter plate was set to an isothermal no-slip wall. Isothermal was chosen so as to not influence the boundary layer development through thermal fluctuations. The boundary condition file used for this flow scenario can be found in Appendix A.

3.4   Job File

The job file is the scripting that initializes the flow solver. Within it are the commands which allow for running it parallel and an input file containing the solver parameters. The major things to note here are the run conditions and the reference parameters. The solver run conditions were set to Laminar Navier-Stokes with 2000 iterations. Time accuracy of the solver was turned off and a large CFL(CFL=10^6) was used to have the time scale adjust to allow the flow to develop quickly to a representative field. 2000 iterations were chosen so as to allow this flow to converge to representative turbulent field. The resultant flow field represents a snapshot of what a numerically resolved field should resemble, but has not used specified local time-stepping for continual flow evolution. The spatial resolution was set to second

Table 1. Flow Reference Parameters

Parameter	Value
Refrence Pressure (P_o)	$P_o = 101325 Pa$
Refrence Temperature (T_o)	$T_o = 288.15 K$
Refrence Top Inlet Mach Number ($M_{1,\infty}$)	$M_{1,\infty} = 0.6$
Refrence Bottom Inlet Mach Number ($M_{2,\infty}$)	$M_{2,\infty} = 0.1$

order while the temporal resolution was set to first order because the purpose is to get a steady-state flow field. The job file used for this flow scenario can be found in Appendix B.

3.5 Fluid Solver

AVUS was used for the CFD work for this scenario. AVUS is an Euler/Navier-Stokes solver, was used to obtain solutions on these grids. AVUS is an unstructured, cell-centered, finite-volume, Godunov-type solver that uses least-squares gradient reconstruction and limiting for second-order spatial accuracy, and second-order, point-implicit time integration. [7; 16] It handles two and three dimensions, arbitrary cell types, and has been efficiently parallelized using Message Passing Interface (MPI). AVUS was used because of previous successful work in this type of research, and the author's familiarity with the program. For AVUS to work it must first be compiled for the parallel processing enviornment of the computational resources being used. AVUS was compiled on the Linux clusters in-house at AFIT. The job file contains all the scripting required to run AVUS on the AFIT clusters.

3.6 Fluid Computation Results Interpretation

At the completion of the flow solver, an intermediate post-processing step is completed to determine the completion and convergence to a completed representative flow field that is steady state. The first step is to examine the completed flow field

using a flow visualization package. Fieldview is an example of a software which can do this. The grid, boundary conditions, and the resultant data are loaded into the software. This is useful in that it provides a visual diagnostic tool to examine the flow field for any errors or problematic behavior. If there are problems it may be necessary to adjust the solver inputs or grid/boundary files to correct for these problems.
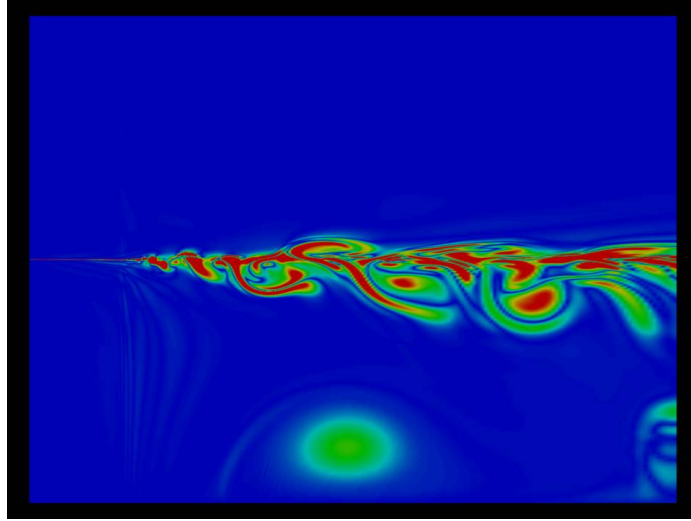
Figure 12. Computed Flow Field Vorticity Magnitude
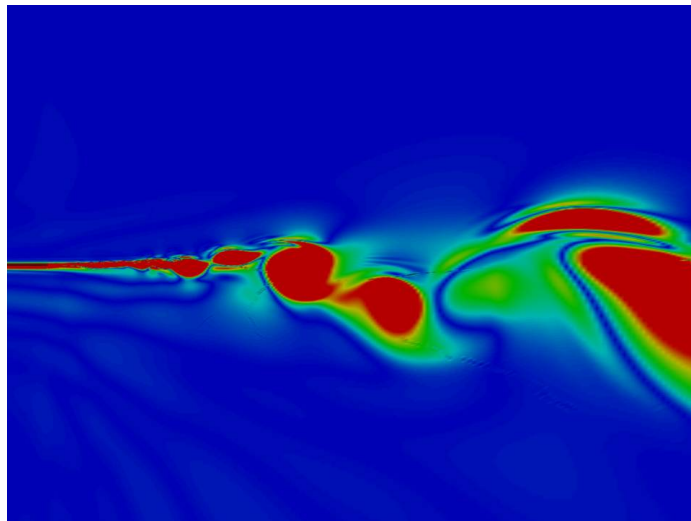
Figure 13. Zoomed in View of the Vorticity Magnitude at the end of the Splitter Plate

Figure 12 provides a view of the converged flow field vorticity magnitude used for this flow scenario. In Figure 12 there is some noise present in the downstream boundary and what looks like a bubble in the lower half, midway through the flow field. This could be sources introduced by the boundary or grid resolution. However, these artifacts were ignored because it was outside of the region of interest for the analysis. Figure 13 gives a more in depth look at the vorticity at the end of the splitter plate (the area of interest). It is evident to note that there is very strong circulation at the end of the plate which is expected. It is also evident that the resolution seems to be good enough to be capturing the eddy structures coming off the plate.

Convergence is determined by analyzing the trends in iteration residuals which AVUS generates as a secondary output. Figure 14 shows the residual convergence trend for the test case. The residual started to level off at about 1500 iterations. It appears to still be decreasing, however the trend suggest that it should be converged to point where further solver iterations will provide only marginal improvements to the flow field solution data. The Y+ is a non-dimensional representation of the wall spacing. For turbulent cases Y+ needs to be as close to one as possible depending on the boundary conditions. Figure 15 is the convergence trend for Y+ for this case as generated by AVUS. It appears to be settling around a Y+ in the low forties. This means that this grid will need to be resized to be used in generating turbulent Navier-Stokes solutions. Here Y+ is used as a diagnostic tool to check for convergence.

3.7 Exporting Flow Data

Following the determination of a converged steady-state laminar shear layer flow field, it is important to get the actual data values calculated from the CFD solver. The Blacksmith utility code developed for use with AVUS grids and results has the capability of generating this geometric data and their corresponding flow parameter

values in a formatted tabular file. It is this file that is imported into the developed optical parameterization algorithm.
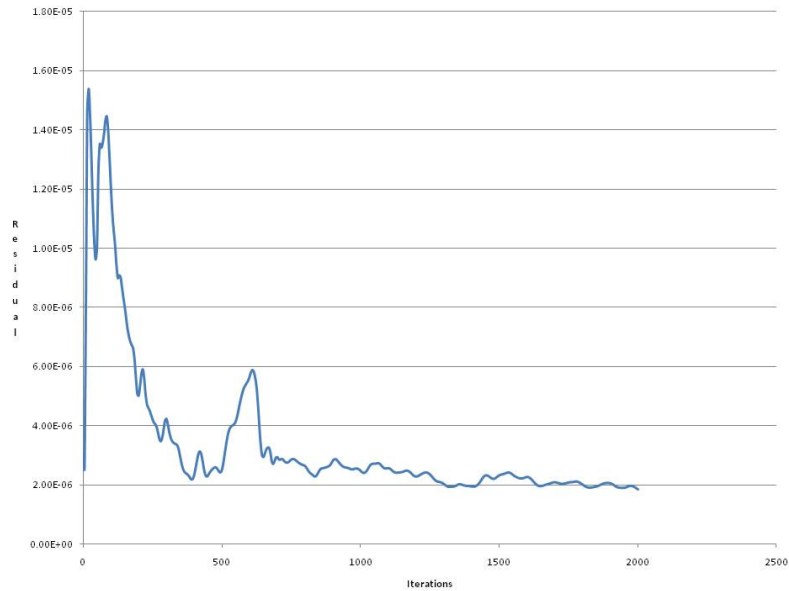
Figure 14. CFD Solution Residual Convergence Trend
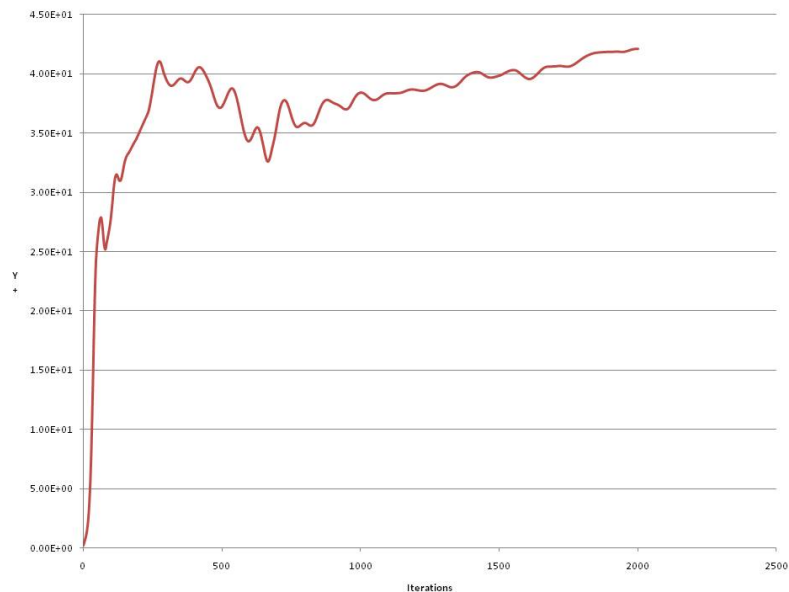
Figure 15. CFD Solution Y+ Convergence Trend

3.8 Optical Parameterization Algorithm

A Matlab code was developed for calculating the parameters needed for the analysis for this study. The algorithm reads in the flow data and generates a focused mesh of this data for the area of interest. It then calculates numerous optical parameters discussed in Chapter 2 for the development of structure functions and the corresponding structure constants. This algorithm can be found in Appendix C.

It is important to highlight here some of the defining values, area of interest, and path defintions. Table 2 provides a list of some of the optical parameter values used in the approach. The region this analysis was conducted on was a $1m \times 1m$ box centered on the end of the splitter plate ($X = 0$ is the end of the splitter plate). A uniform mesh was constructed in this box using a spacing of 0.001 giving 1001×1001 data points for the calculations. The reference point for the calculation of the structures was set to the spatial values set at $X = 0.5m$ and $Y = 0m$ which is the center of the mesh. Because the structure functions are calculated from spherical coordinates it was necessary to calculate the radial distances from the mesh center. A tolerance was used in the radial distance determination for calculating the structure functions. A plane wave was assumed for the beam as this is a 2-D flow field. For the path dependent integrals and aperture averaging the Y-direction represents the propagation direction and the X-direction represents the aperture face. A visualization of this approach can be seen in Figure 16.

3.9 Output

The data is calculated in Matlab. Matlab has great plotting capabilities and was used to generate data plots for interpretation. A more in-depth presentation of this can be found in Chapter 4.
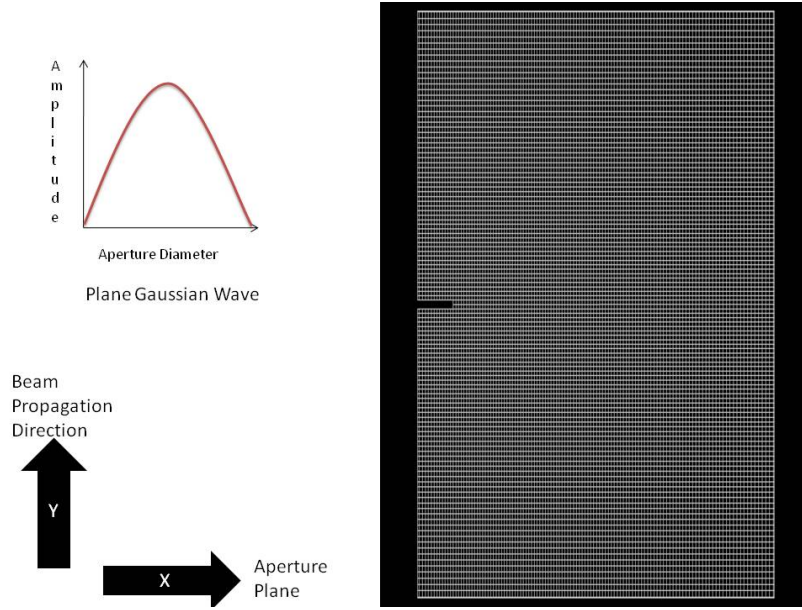
Figure 16. Parameterization Algorith Assumptions Visual

Table 2. Reference Data for Parameterization Algorithm

Beam Waist (w_o)	$w_o = 0.5m$
Amplitude Peak (A_o)	$A_o = 1$
Wavelength (λ)	$\lambda = 1m$
Reference Density (ρ_o)	$\rho_o = 1.221\frac{kg}{m^3}$
Gladstone-Dale Constant (K_{GD})	$K_{GD} = 2.25 \times 10^{-4}\frac{kg}{m^3}$
Radius Tolerance	$tol = 0.0005m$
Grid Spacing $(\Delta x, \Delta y)$	$\Delta x = 0.001m, \Delta y = 0.001m$
Radial Stepsize (Δr)	$\Delta r = 0.001m$

36

IV. Results and Analysis

Chapter 4 is a compilation of the results obtained for defining the stochastic optical paramters for this 2-D laminar shear layer for the splitter plate geometry. The results begin with an analysis of the flow field, with regard to the actual Reynold's Number within the mixing layer and require scale resolution. This leads to the the development of the local refractive indicies and OPD's with a comparison between the two methods used for calculating the refractive index in these developments. This is followed by the presentation of the results of the structure function development and the constants calculated assuming the $r^{\frac{2}{3}}$ power law including a discussion on deviations from expectations and reasonableness of the numbers calculated.
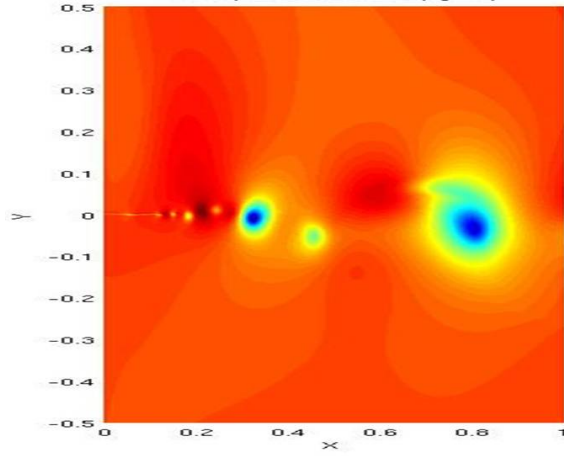
Figure 17. Area of Interest Density Mesh
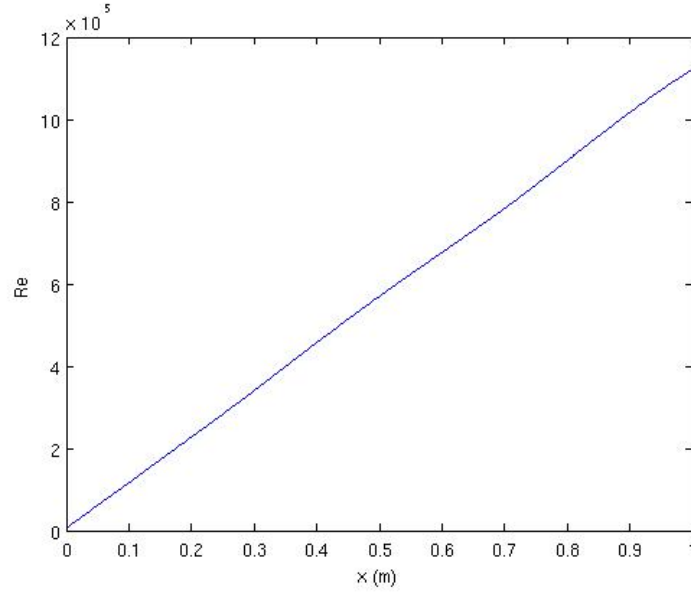
Figure 18. Streamwise Reynold's Number within the Mixing Layer for the Area of Interest
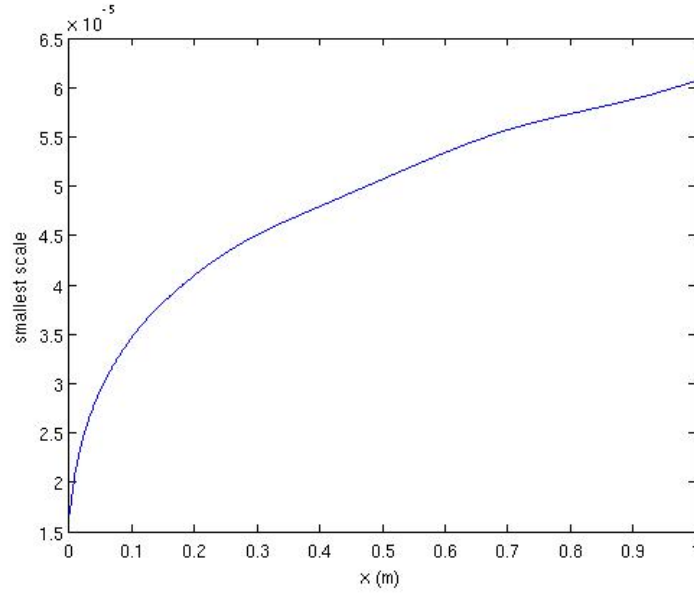
Figure 19. Streamwise Smallest Scale Size Resolution within the Mixing Layer for the Area of Interest

4.1 Flow Field in Area of Interest

As described in Chapter 3 the area of interest is confined to $1m \times 1m$ box centered at the end of the splitter plate. Density is the primary flow parameter in determining

the local refractive indicies. Figure 17 is a view of the local densities within this area of interest as meshed by Matlab. This figure gives a good view of the eddies flowing from the end of the plate with regard to variations from higher density (red) to lower density (blue).

The flow field seems to capture some of the large scale features, but doesn't really provide any insight into if the flow in the mixing layer is turbulent or not. The best way to investigate this is to calculate the Reynold's Number along the streamwise direction within this area of interest. The Reynold's Number is calculated using Equation 1. The flow speed for this analysis is calculated by the following equation where the Mixing Layer Flow Speed(ΔU) is the average of the upper freestream velocity ($\bar{U}_h$) and the lower free stream velocity ($\bar{U}_l$).

$$\Delta U = \frac{\bar{U}_h - \bar{U}_l}{2} \tag{17}$$

The length scale($L(x)$) used is the half width of the mixing layer which is found by taking the average in difference between the Mixing Layer Flow Speed (ΔU) and the Lower Freestream Velocity ($\bar{U}_l$).

$$L(x) = \frac{\Delta U - \bar{U}_l}{2} \tag{18}$$

The streamwise Reynold's Number can be found in Figure 18. The Reynold's Number grows linear within this area of interest and quickly approaches 10^5 which shows that this mixing layer is turbulent and should have a Kolmogorov like distribution of scales.

However, the grid was constructed assuming a laminar shear layer so it is necessary to compute what the smallest resolution is required to capture the smallest eddy

scales. The inner scale $(l(x))$ is computed by using the following relation.

$$l(x) = \frac{L(x)}{(0.1Re^{\frac{3}{4}})} \tag{19}$$

This result is plotted in Figure 19. This shows that the smallest scale is on the order of $10^{-5}m$. However the smallest scale size for this grid is $10^{-3}m$. This means that while the mixing layer is turbulent with regard to Reynold's Number the scale sized used may not effectively capture the entire distribution of scales, which may limit the feasibility in the interpretation of the results. However, there are sufficient large scale eddies present which have a more dominant effect on optical beam propagation.

4.2 Refractive Index and OPD

Using the density mesh presented above the local refractive indicies were calculated and meshed using the two methods described in Chapter 2: Edlen (Equation 2) which includes wavelength and Gladstone-Dale (Equation 3). Figures 20 and 21 show the mesh calculated using the above equations. A quick comparison of the two figures reveals that the two fields are indistinquishable. This suggests that at 1 micron wavelength the calculations are very close. The other observation that can be made is that the index variation maps very closely to the eddies in the flow as expected since they are density dependent and are evident in Figure 17.

The local OPD is calculated from the local OPL's generated by the local refractive indicies as described in Equation 6. Figures 22 and 23 show the OPD mesh for the respective fields. Much like the refractive index meshes these are indistinquishable which is consistent with the fact that the calculations are based on the refractive index. Figure 24 provides a sample of the OPD at the top of the box along the streamwise direction for the two different OPD's. They seem to match very well.
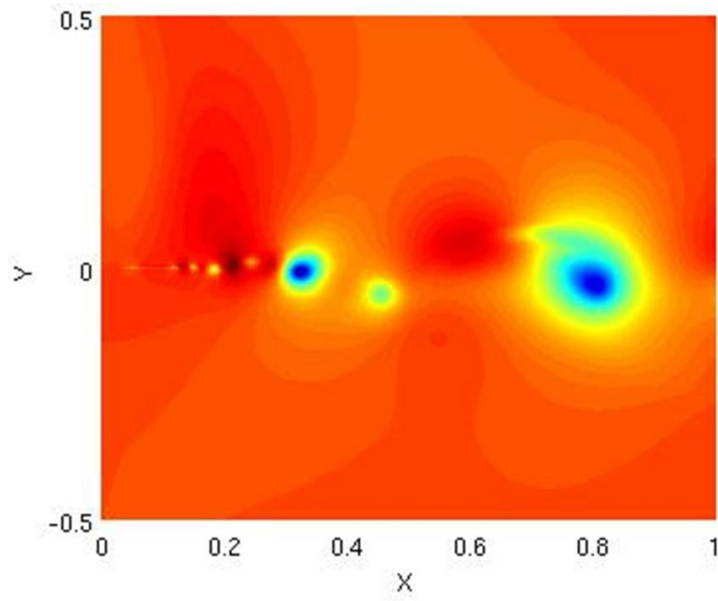
Figure 20. Local Refractive Index Using Edlen Formula
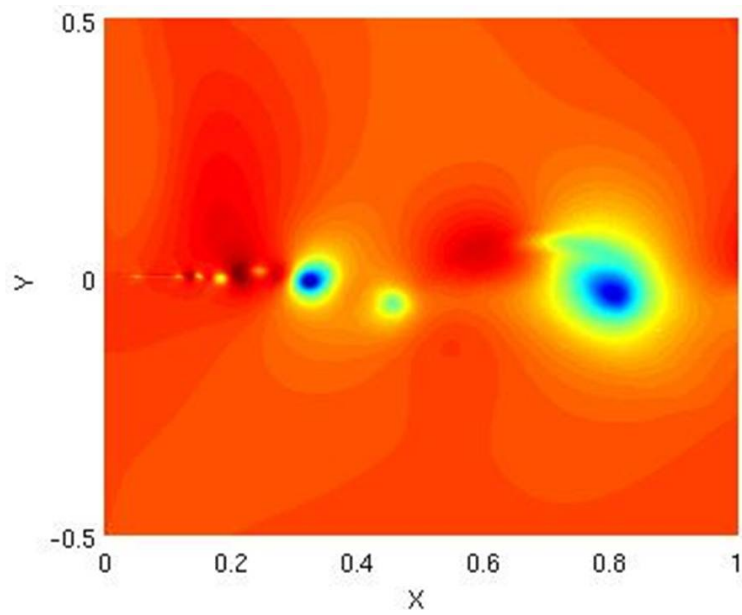
Figure 21. Local Refractive Index using Gladstone-Dale

41
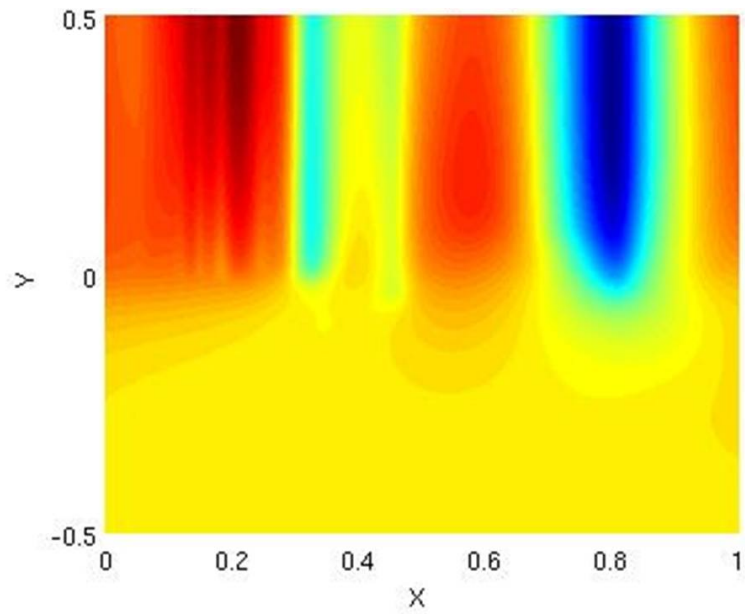
Figure 22. Local OPD from Edlen Refractive Indicies
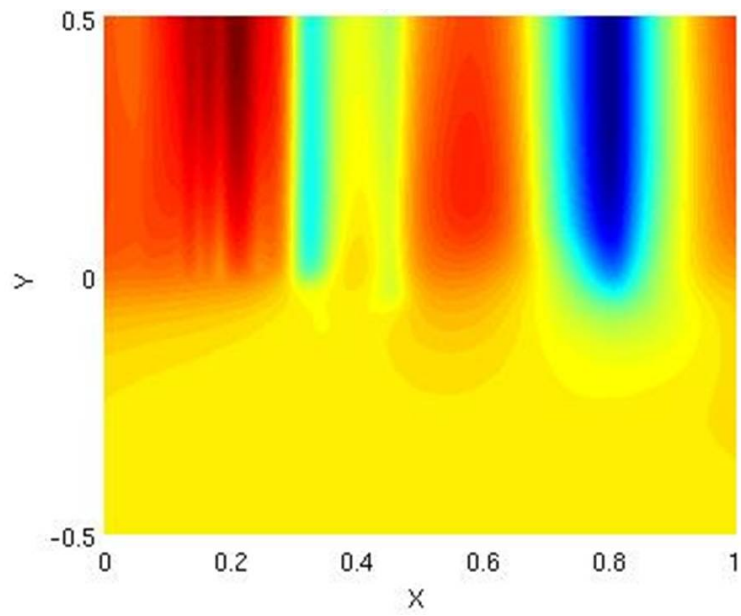
Figure 23. Local OPD from Gladstone-Dale Refractive Indicies
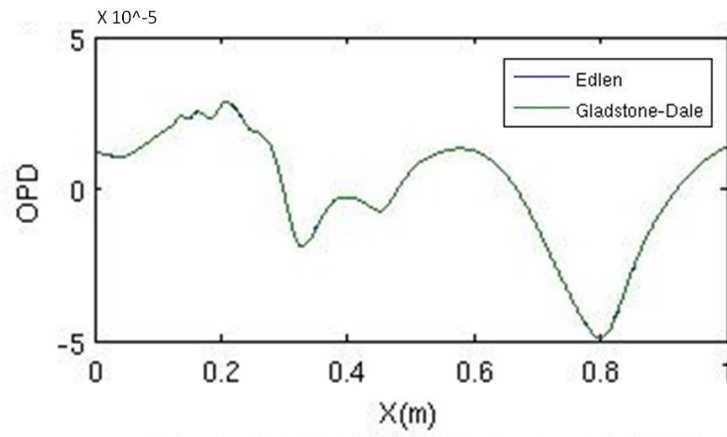
Figure 24. OPD Comparison between Refractive Index Methods
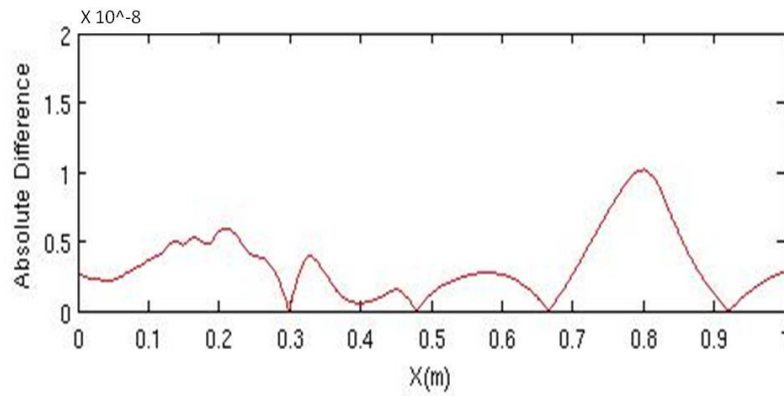
Figure 25. OPD Absolute Difference of Methods

Figure 25 provides an absolute difference in the two values. The difference between them on the order of 8 decimal places which suggests there is negligible difference in

43

the two refractive index methods for this wavelength. This provides a reasonable argument for choosing a single method for these calculations at this wavelength. However, both methods were used throughout this algorithm so as to ensure similarity of methods.

4.3   Structure Functions and Constants

The first structure function calcuted was $D_n(r)$ using the method described in Equation 9 directly from the flow field data. The results from this calculation can be found in Figure 26. The data trend should resemble Figure 6 in that it should go rapidly to zero as the separation distance (r) gets smaller. This is not what is seen here. This could be a result of a lack of datapoints for sampling at the smallest scales. Figure 27 gives the number of datapoints sampled for all the separation distances for the averages. This gives some indication of the resolution limiting at the smallest scales which prevents the trend from happening as expected. At the largest scales there appears to be some oscillation in the structure function. These could be due to the selection of the reference point in that there may be stronger variations in the refractive index respective to that reference point. Because this was a single timestep and a single reference point there could be a lack of sampling data in these regions inducing these oscillations. This might be able to be corrected using various references and averaging or using time averaged data for a time evolving flow. This also demonstrates that this flow is anything but isotropic and homogeneous. However these limitation could be due to the coarseness in the grid resolution which can't capture the smaller scale eddies.

From the refractive index structure function, $D_n(r)$, the C_n^2 was calculated using the $r^{\frac{2}{3}}$ power law. This can be seen in Figure 28. These points are the circles(Edlen) and x(Gladstone-Dale). These C_n^2 values represent what they would be if Kolmogorov
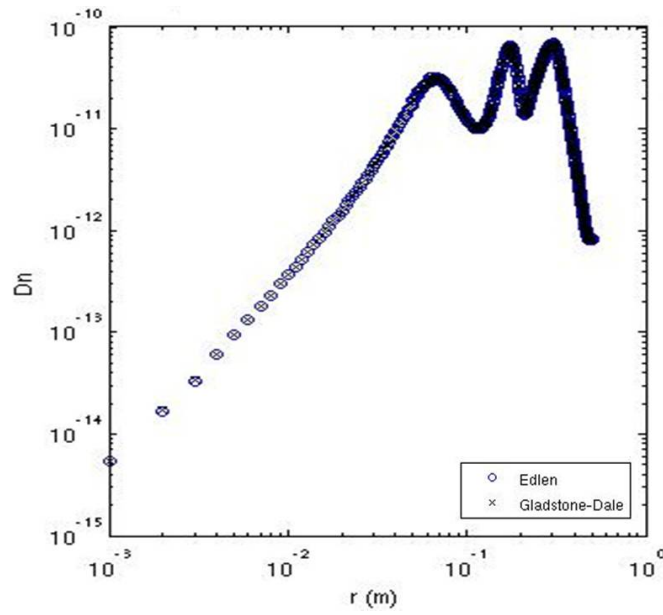
Figure 26. Refractive Index Structure Function as Calculated from Varying Refractive Index's in the Flow Field
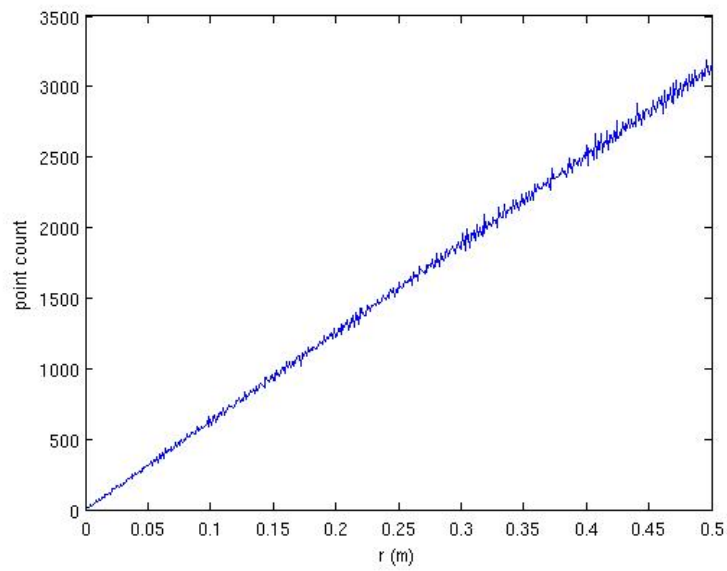
Figure 27. Number of Data Points Sampled for Corresponding Separation Distance

was assumed using the $r^{\frac{2}{3}}$ power law. The first thing to note is that this not a constant using the $r^{\frac{2}{3}}$ power law which suggests that the aero-optical flow is non-Kolmogorov. The other thing is the range of C_n^2's is between 10^{-12} and 10^{-10} which is higher than expected for definitions of atmospheric turbulence(Typical Range: $10^{-17} < C_n^2 < 10^{-12}$). This seems to suggest that this particular flow field is non-Kolmogorov. Again though this was a single data field for a specific case. Time averaged data or varied reference points, a more finely resolved grid, or a turbulent Navier-Stokes produced case may yield more Kolmogorov like turbulent profiles.
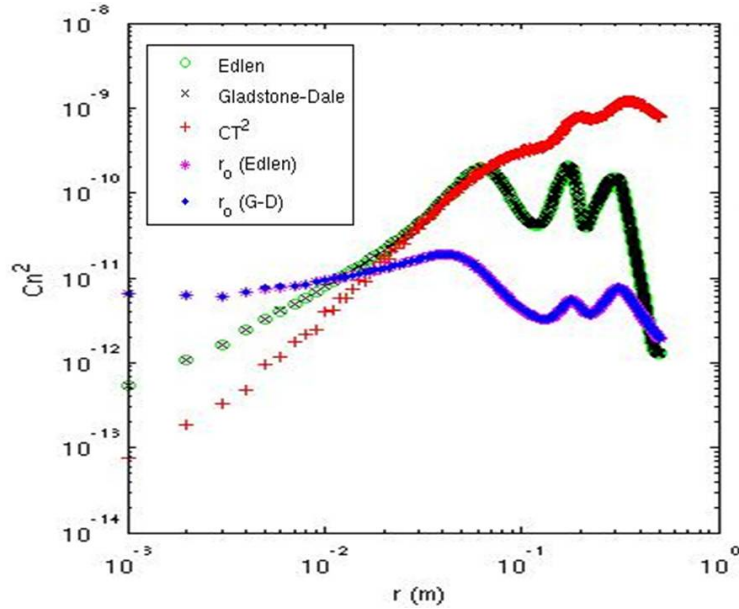
Figure 28. Calculated Structure Constant (C_n^2) from $D_n(r)$ using $r^{\frac{2}{3}}$, C_T^2 from Flow Field, and r_o from the Flow Field

Figure 28 also compares various other methods for calculating the C_n^2 from other parameters. The red + signs represent the C_n^2 values found by assuming Kolmogorov distribution in the flow field for the local temperatures. C_T^2 was found by constructing the temperature structure function ($D_T(r)$). This is then used to calculate C_n^2 using Equation 12. The asterisks and diamonds is the C_n^2 as calculated using Equation 15 from which the r_o values were calculated from the field using Equation 13.

What is interesting to note is the regions where the trend is coincidental. Building C_n^2 from C_T^2 overlaps in the range of $0.01m - 0.1m$ which is within the theoretical atmospheric inertial subrange. It is also interesting to note that using thermal gradients for Kolmogorov Theory corresponds with the flow field derived parameters over a longer range in that atmospheric analysis use thermal gradients to determine the parameters. The agreement by calculating C_n^2 from r_o has a much smaller range $(0.01m - 0.02m)$, yet is also within the theoretical atmospheric inertial subrange.

Figure 29 presents the computation of the Fried Parameter for two methods. The first two lines(Edlen and Gladstone-Dale) represent constructing the Fried Parameter based on the Phase and Amplitude structure functions as found using Equation 13. The second two lines (C_n^2) represent the calculation from C_n^2 values found using the $r^{\frac{2}{3}}$ power law with $D_n(r)$. Again the values assume a variable range rather than a definate value. However from a separation distance range of $0.01m - 0.02m$ there seems to be some agreement for $r_o \approx 0.05m$ which is a reasonable value for the Fried Parameter. It is also interesting to note the differences between the two methods. This can be seen in Figure 30. There is a range of values from which they differ however there is an average difference of about $5cm$. That means that for sizing r_o there is almost insignificant difference in value between a statistical representation and the actual flow field derived values for the purposes of system design for Adaptive Optics.

Another method of comparison of the results is the corelation of the phase structure function $(D_\phi(r))$ calculated from the field and the $D_\phi(r)$ from the C_n^2. These results can be seen in Figure 31. The Edlen and Gladstone-Dale points represent the values calculated from the flow field. The C_n^2 lines are derived from using the values calculated using Kolmogorov. From this figure the discussion relative to the function trend presented above for $D_n(r)$ applies here.
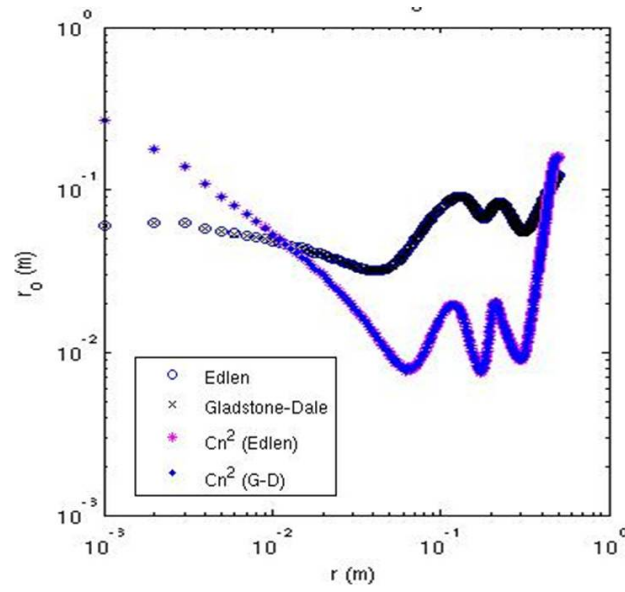
Figure 29. Calculated Fried Parameter (r_o) from $D_\phi, D_{ln(A)}$ and C_n^2
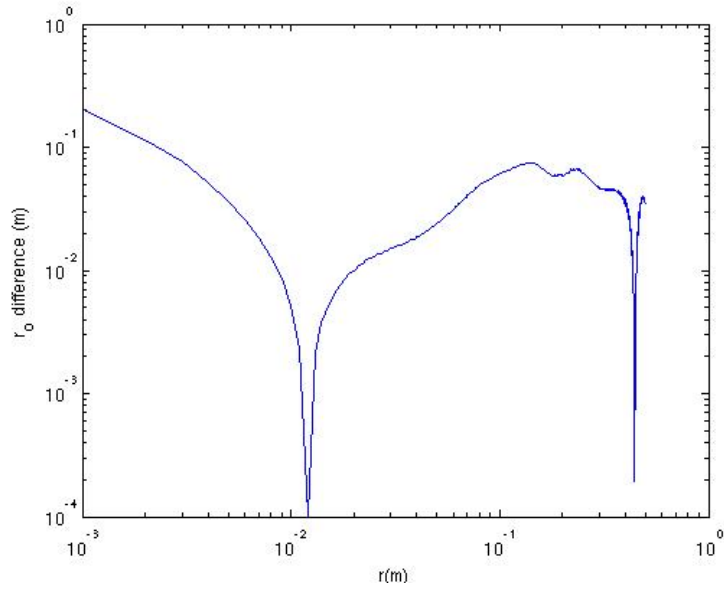
Figure 30. Calculated Fried Parameter (r_o) Difference between Methods
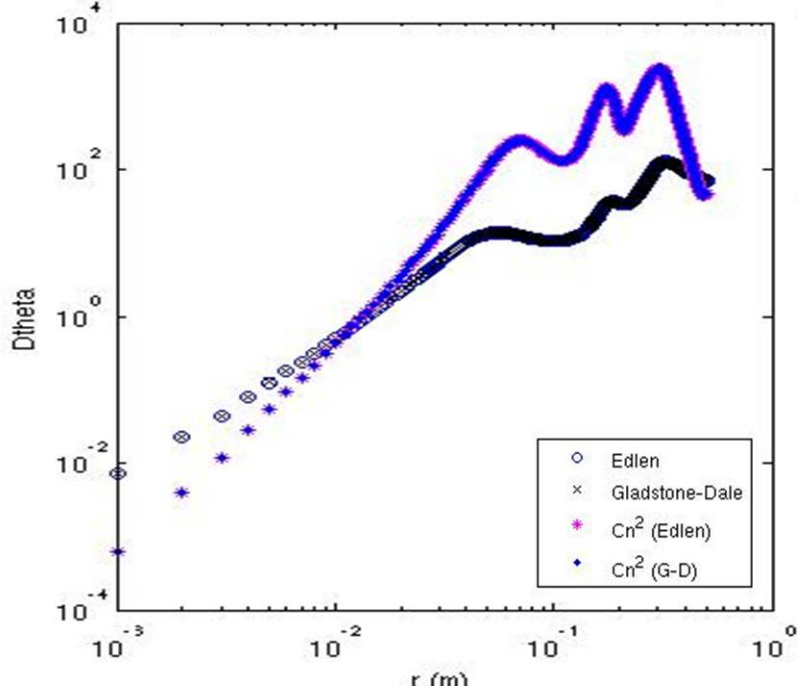
Figure 31. Phase Structure Function Comparison $(D_\phi(r))$ as found from Flow Field and Kolmogorov Derived C_n^2

Table 3 is a synopsis of the interesting details from these results. This $0.01m - 0.02m$ range is very interesting in its repetition and the fact that it is within the atmsopheric inertial subrange. This may be purely coincidental though without further grid refinement to ensure capture of the smallest turbulence scales. While there are major quantifiable differences between the methods for this shear mixing layer, this suggests that further scenarios would need to be conducted to draw any relevant conclusions on if this is purely coincidental or has some applicable ramifications.

Table 3. Summary of Interesting Parameterization Data

Comparison	Agreement Value/Range
r_o	$r_o \approx 0.05m$
C_n^2	$10^{-12} - -10^{-10}$
$C_n^2(r)$ from Flow to $C_n^2(r)$ from C_T^2	$0.01m < r < 0.1m$
$C_n^2(r)$ from Flow to $C_n^2(r)$ from r_o	$0.01m < r < 0.02m$
r_o from Flow to r_o from C_n^2	$0.01m < r < 0.02m$

V. Conclusions

This chapter begins by providing a cursory summary of the results. It then outlines opportunities for improvement to the existing methodology. It concludes with suggestions regarding future work in the area of research.

5.1 Results Summary

Siegenthaler et al concluded that aero-optic flows are non-Kolmogorov like because they suggest that centrifigal forces associated with the eddies are more dominant than the thermal variations in these eddies. Stochastic methods work in the atmosphere because temperature gradients are the primary force behind inertial subrange turbulence paired with high Reynolds numbers to make Kolmogorov theory applicable. In aero-optical flows there are temperature fluctuations in the eddies, but the primary source of turbulent kinetic energy is in the inertia of the whirling flow, where the whirls produce density and refractive index gradients via centrifigual effects which seems to be consistant with what Siegenthaler et al were suggesting. Figures 28 shows that the Kolmogorov derived C_n^2 and C_n^2 from C_T^2 have a larger range of overlap which suggests that temperature gradients are the dominant parameter in scaling for turbulence strength using Kolmogorov. When calculating C_n^2 from a flow field characteristic r_o there is much less agreement which suggests that thermal gradients were not the dominant parameter. It doesn't make a case for what parameter, but Siegenthaler et al hypothesize centrifugal force seems to be a relevant factor. In light of these discussions, the 2-D shear mixing layer aero-optic like flow was not Kolmogorov despite the fact that the mixing layer appears to be turbulent. This could be a result of not having enough grid resolution to capture the smallest eddy scales.

However, stochastic methods might serve as a useful way to derive system design

parameters for Laser Weapons Systems. The Fried Parameter is often used to determine the acuator numbers and scaling for the Adaptive Optics system. By comparing Kolmogorov based analysis with that of flow field measurement there were differences, but these differences were small (approximately $5cm$). While this isn't insignificant, it suggests that a stochastic method provides a reasonable ballpark figure for determining the Fried Parameter for a given system. Statistical methods may not be the most accurate or complete descriptions but may provide a good enough representation for an aero-optical flow over an Airborne Laser Weapons System.

Based on the results presented in Chapter 4, this particular aero-optical flow (2-D shear mixing layer) does not seem to have Kolmogorov like defining parameters which could be a result of not capturing the full distribution of eddy scales. The structure functions do not seem to behave with the expected trends. The structure constant is not a constant and it's range of values is higher than what is expected for the turbulent atmosphere. However there are ranges where the data seems to reinforce the values derived. This gives some providence in investigating deeper. Some opportunities for improvement this are found in the next section.

5.2   Opportunities for Improvement

The first opportunity for improvement is to choose one index of refraction calculation. The results show that there is very little difference between the Edlen and Gladstone-Dale methods at the near-IR wavelengths. In light of this, selecting and using Edlen would be sufficient. It accounts for both wavelength and density variations.

The second opportunity is to compare multiple reference points for the structure function development. This ignores the feasibility of assuming the flow is isotropic but may provide some smoothing to the structure functions that may make them

51

more Kolmogorov. The isotropic nature may be restored if these various reference point parameters are averaged.

The third opportunity is to improve the resolution of the mesh. This would potentially better smooth out the data as well as provide more data points. However, this would be a more intensive operation computationally. It would require rebuilding the fluid grid to capture more flow data, which would increase computational requirements and time. The additional data would also require more work from Matlab to generate the meshes from which the parameters are developed from.

5.3 Future Research Opportunities

This investigation was confined to a very isolated case. A 2-D shear mixing layer case provides a good opportunity to explore the details of the methodology developed for this research. However, it is apparent that there are opportunities to improve this methodology. Depending on the feasibility or the direction of implementing those opportunities, it would be important to have an idea of how to extend this methodology for more relevent scenarios.

The next logical step is to make this 2-D shear mixing layer fluid field evolve with time and what effects unsteadiness in the flow has on this parameterization. This can begin with the initial solution used for this project and take sample data from several timesteps as it evolves. The subsequent logical step would then to make a 3-D laminar flow field. The more interesting case would then be a 3-D turbulent cases which may behave more inline with Kolmogorov Theory. The problem with a 3-D turbulent case would be the increase in computational requirements. The 2-D grid for this research included 500,000 grid cells. A 3-D grid would have $n \times 500,000$ more cells depending on the minimum gridspace required. That number would likely be much higher in order to capture the boundary layer development for a turbulent case

as this grid had a Y+ ten times greater than a viable Y+ for a turbulent case.

The ultimate goal for this methodology is for it to be expanded onto a turret configuration. A turret would provide an operational configuration for developing aero-optical turbulence and determining the Kolmogorov relation feasibility. This would also introduce a lot more complexity in the development of the grid and computational requirements to apply this methodology. However, it would make a more definitive conclusion regarding the Kolmogorov-like relationship of an aero-optical flow. If this scenario had a Kolmogorov-like aero-optical turbulence, system design could be simplified by applying simple statistical methods for accounting for turbulence, versus extensive simulations of chaotic aero-optical turbulence fields.

Appendix A. Boundary Condition File

```
####################################################

   Boundary Condition Specification File for:

   'Replace this line with a title'

####################################################
 9
top_inlet
Source
Riemann Invariant
 P-Stat    T-Stat   K   Omega   Mach   Axis End Points   Swirl (A,B,C)
101325.0  288.15  -1.   -1.    0.6   0. 0. 0.   1. 0. 0.    0. 0. 0.
No
##################################################
 10
top
Solid Wall
Slip
No
##################################################
 11
outflow
Farfield
Modified Riemann Invariant
 P-Stat    T-Stat     K     Omega     Mach    Alpha     Beta
 -1.      -1.      -1.      -1.      -1.     -370.     -370.
###################################################
```

```
 12

bottom

Solid Wall

Slip

No

##################################################

 13

bottom_inlet

Source

Riemann Invariant

 P-Stat    T-Stat    K    Omega    Mach    Axis End Points    Swirl (A,B,C)

101325.0  288.15   -1.    -1.     0.1    0. 0. 0.    1. 0. 0.     0. 0. 0.

No

##################################################

 14

splitter_plate

Solid Wall

Isothermal No Slip

 Wall Temperature

    288.15

No

##################################################
```

Appendix B. AVUS Job File

```
#!/bin/bash

#########################

# Queue Options

#########################

#PBS -l nodes=6:ppn=2

#PBS -M james.bowers@afit.edu

#PBS -m abe

#PBS -j oe

#PBS -V

#

#echo Working directory is $PFS_O_WORKDIR

cd $PBS_O_WORKDIR

#########################

# Script Banner

#########################

echo -e ""

echo -e "====================="

echo -e " AVUS Job File Script "

echo -e "====================="

#########################

# AVUS - File names

#########################

export GRIDNAME=spltplt_2D_laminar;

export BCNAME=spltplt_2D_laminar;

export RESULTNAME=spltplt_2D_laminar;
```

```
export TAPNAME=;

#########################
# AVUS - File paths
#########################
#export AVUSLOC=${HOME}/avus/bin;

export AVUSLOC=${HOME}/avus;

export JOBLOC=${HOME}/mydocs/runschtuff;

export GRIDLOC=${JOBLOC};

export BCLOC=${JOBLOC};

export SCRATCH=${PBS_O_WORKDIR}/spltplt_2D_laminar;

export RESULTLOC=${SCRATCH};

export TAPLOC=${SCRATCH};

#########################
# AVUS - Executable Spec
#########################
export MACHINE_ARCH="linux";     # linux | macosx | etc...

export PRECISION="double";       # single |double

#export RUNSCRIPT="avus.linux.dp"; # AvusRUN | AvusRUN_ibm

export RUNSCRIPT="AvusRUN"; # AvusRUN | AvusRUN_ibm

#########################
# MPI - Run command
#########################
export RUN="mpirun"

#########################
# Clean scratch directory
cd $SCRATCH/
```

```
rm -f avus AvusIN* AvusOUT* fort.* *.shutdown

#########################

cat > $SCRATCH/$RESULTNAME.inp << EOF

********************************************************

                TITLE

********************************************************

 Shear Flow Turbulence DES    24 Nov 2009

********************************************************

         INPUT FILE CONTROL PARAMETERS

********************************************************

 START OPTION (1=INITIAL RUN, 2=RESTART, 3=RESTART & RECALC WALL DIST)

     1

 NO. PROCESSORS     GRID & INTERSECTION FILE FORMAT (0=UNFORM, 1=FORM)

    10    0

 SPLITTING PROCS    PROVIDE FLOW DATA? (0=NO,1-11=YES)

    -1                   0

********************************************************

         OUTPUT FILE CONTROL PARAMETERS

********************************************************

 CREATE PICTURE FILE? (0=NO,1-9=YES)  FORMAT(0=UNFORM, 1=FORM)

     6                        0

 CONVERGENCE FREQ.        RESTART FREQ.   MOVIE TAP FREQ. PIX FREQ.

     5                      -1              -1         500

********************************************************

         ALGORITHM PARAMETERS

********************************************************
```

```
EQUATION SET (1=EULER, 2=LAMINAR N-S, 3=TURBULENT N-S)
         2
TURBULENCE MODEL (1=SPALART,2=Spalart-DES,3=MentorBSL,4=MentorSSTT)
         2
SPATIAL ACCURACY (1 OR 2)   TEMPORAL ACCURACY (1 OR 2)
         2                        1
THETA (0.5-1.0)
         1.00
RHS IFLUX(1=G&G) LSTSQ.WTS(0=OFF,1=ON) LIMITER(0=OFF,1=B&J,2=Venk)
         1                          0                   2
ITERATIVE MATRIX SOLUTION SCHEME (1=JACOBI, 2=GAUSS-SEIDEL)
         2
NO. ITERATIONS (SWEEPS) OF ABOVE MATRIX SOLUTION SCHEME
        32
INVISCID JACOBIAN DDF     VISCOUS JACOBIAN DDF
        0.1            0.1
CFL        TIME STEPS     NEWTON SUB-ITERATIONS
1.e+6       2000                  1
TIME ACCURATE?              REQUESTED TIME STEP
     0                        -1.
******************************************************
     REFERENCE CONDITIONS & PHYSICAL CONSTANTS
******************************************************
UNITS (1=MKS, 2=CGS, 3=FOOT-SLUG-SEC, 4=INCH-SNAIL-SEC)
   1
MACH NO.   ANGLE OF ATTACK   ANGLE OF SIDESLIP
```

```
    0.        0.                  0.

 STATIC PRESSURE     STATIC TEMPERATURE

       101325.0                  288.15

 GAMMA     GAS CONSTANT     PRANDTL NUMBER     GRAVITY

  -1.        -1.                  -1.            0.

 *******************************************************

                 INITIAL CONDITIONS

 *******************************************************

 MACH NO.      ANGLE OF ATTACK      ANGLE OF SIDESLIP

  0.           0.                  0.

 STATIC PRESSURE     STATIC TEMPERATURE

       101325.0                  288.15

 TURBULENT KINEMATIC VISCOSITY RATIO

       -1.   -1.

 *******************************************************

                 GEOMETRY PARAMETERS

 *******************************************************

 COORDINATE SYSTEM (1=FLO57, 2=PANAIR, 3=AXI-SYMMETRIC)

     1

 AXISYMMETRIC FORCE ACCOUNTING

    -1

 REFERENCE AREA

     0.0

 X,Y,Z COORDINATES OF MOMENT REFERENCE POINT

   0.0 0.0 0.0

 REFERENCE LENGTHS FOR MOMENTS ABOUT X-,Y- AND Z-AXIS
```

```
      0.0 0.0 0.0

*******************************************************

           NONINERTIAL REFERENCE FRAME

*******************************************************

 OMEGA(1:3) - NON-INERTIAL ROTATION VECTOR (RAD/S)

     0.00    0.00     0.00

 OMEGACNTR(1:3) - CENTER OF NON-INERTIAL ROTATION

     0.00    0.00     0.00

 INITIAL ROTATION (0=NONE,1=USE OMEGA,2=USE INITOMEGA)

     0

 INITOMEGA(1:3) - INITIAL NON-INERTIAL ROTATION (RAD/S)

     0.00    0.00     0.00

 INITOMEGACNTR(1:3) - CENTER OF INITIAL ROTATION

     0.0     0.0      0.0

*******************************************************

           FLUID VOLUME MESH DEFORMATION

*******************************************************

 MESH DEFORMATION METHOD (0=NONE, 1=VOLDEF, 2=DYNMESH)

     0

*******************************************************

           END OF INPUT INFORMATION

*******************************************************

EOF


#-----------------------------------------------------

# AvusRUN script argument list:
```

```
#
#  1 - AVUS input file name
#  2 - AVUS output file name
#  3 - precision switch
#  4 - grid file name
#  5 - old restart file name
#  6 - new restart file name
#  7 - picture file name
#  8 - tap location file name
#  9 - shutdown file name
# 10 - performance file
# 11 - bl trip file name
# 12 - bc file name
# 13 - overwrite flag
# 14 - machine type
# 15 - '-mdiceargs' (optional:only when run from MDICE)
# 16 - string of mdice args (optional:only when run from MDICE)
#----------------------------------------------------
# Available precision:
# single, double
#
# Available machine types:
# ibm,sgi,t3e
#----------------------------------------------------
#
#
```

```
$AVUSLOC/$RUNSCRIPT \

$SCRATCH/$RESULTNAME.inp \

$RESULTLOC/$RESULTNAME.out \

$PRECISION \

$GRIDLOC/$GRIDNAME.grd \

$SCRATCH/junk.intr \

$RESULTLOC/$RESULTNAME.rst \

$SCRATCH/$RESULTNAME.trst \

$RESULTLOC/$RESULTNAME.pix \

$SCRATCH/$JOBNAME.tap \

$SCRATCH/$RESULTNAME.shutdown \

$SCRATCH/$RESULTNAME.movtap \

$SCRATCH/ramp.trip \

$BCLOC/$BCNAME.bc \

overwrite \

$MACHINE_ARCH \
```

Appendix C. Parameterization Algorithm

Listing C.1. flowoptics.m

```
%% FlowOptics
%Written by: Captain James C Bowers
%Date:  9 Dec 2009
%Summary:  This code uses flow data generated using a CFD solver and
%calculates Statistical Optical Parameters


%%  Data Import
datareadin

%% Pressure Temperature Conversion
ptconv

%% Index of Refraction Calculation
index

%% Allocating data to Grids
datamesh

%% Radius Calculation Mesh
radmesh

%% OPL Calculation Loop
oplcalc

%% OPD Calculation Loop
opdcalc

%% Theta & Amplitude calc
phaseamp

%% Developing Structure Functions
structure

%% Flowfield Data Plotting for Visualization
```

flowviz

metric

Listing C.2. datareadin.m

```matlab
%——————————————————datared.m——————————————————————%
%Reads in result data output by blacksmith for given flow data
%Created by:  James C Bowers  Date:  5 Jan 2010
%Used for pulling the flowdata into arrays for calculations by itself or as
%part of a subroutine in larger code to analyze data for optical
%properties.  jcb 5 jan 2010
%—————————————————————————————————————————————————————————%


%% Clears and Closes any open files and variable used or created in routine
close all
clear fid i tline numptsstr numpts x y rho u v w press kmu


%% Opens Data File for read in and metrics
fid=fopen('/home/afiten3/gap10m/jcbowers/Matlab/data/2D_laminar_data.dat','r');
i=0;


%% Number of Points of Data to input
%While loop goes line by line through header to find the spot in the third
%line of the header which tells the number of data points to pull in since
%there is more lines of data regarding the geometry past the area of data
%that is of interest.

while feof(fid)==0

    tline=fgetl(fid);
    i=i+1;

    %When it hits the third line it pulls the string with the number of
    %data points and then converts it to a number.  This method is specific
    %to the file I am reading in.  May need to be fixed or adjusted with
    %different files.

    if i==3
        numptsstr=tline(26:31);
        numpts=str2double(numptsstr);
        break
    end
```

```matlab
end


%Closes file after getting numpts for read
fclose(fid);


%% Data Read In
%Ignores first 3 lines of data file then stores the following tabular data
%into respective arrays for the number of points (numpts) it should get.

[x,y,rho,u,v,w,press,kmu]=textread ...
    ('/home/afiten3/gap10m/jcbowers/Matlab/data/2D_laminar_data.dat'...
    ,'%f %f %f %f %f %f %f %f \n',numpts,'headerlines',3);


%% Data Clean Up
%Not all of the flow data is useful and will be cleared to free of space
%and clutter of workspace.

clear u v w kmu tline i fid ans numptsstr


% End of Routine
```

Listing C.3. ptconv.m

```
%————————————ptconv.m————————————————————————————————%
%Reads in pressure and density data to create temperature data and then
%converts the pressure from Pascals to mbars.
%Created by James C Bowers Date:  5 Jan 2010
%—————————————————————————————————————————————————————————%
%Inputs:
%numpts = numpts of data from file
%press = pressure data from file
%Outputs:
%temp = temperature data calculated
%—————————————————————————————————————————————————————————%

clear temp i

temp=zeros(numpts,1);  %Initializing temperature array

for i=1:numpts

    temp(i,1)=press(i,1)/(rho(i,1)*287);  %Temperature calculation

    press(i,1)=press(i,1)/100;  %Pressure Conversion

end

clear i

% End Routine
```

68

Listing C.4. index.m

```
%————————————index.m————————————————————————————%
%Routine that take flow data and calculates index of refraction from the
%data at those points.
%Created by James C Bowers   Date: 5 Jan 2010
%——————————————————variables——————————————————————%
%Input Variables
%press = pressure data (called in)
%temp = temperature data (called in)
%rho = density data (called in)
%numpts = number of data points (called in)
%lamda = wavelength in microns (first specified)
%kgd = Gladstone−Dale coefficient (first specified)
%
%Output Variables
%ned = index of refraction using Edlen
%ngd = index of refraction using Gladstone−Dale(density)
%———————————————————————————————————————————————%


clear ned ngd lamda kgd i


%Initializing refractive index grids
ned=zeros(numpts,1);
ngd=zeros(numpts,1);


lamda=1;  % Wavelength in microns
kgd=2.25e−4;  %Gladstone Dale Constant assuming 1 micron wavelength


for i=1:numpts

    %Edlen Index of Refraction
    ned(i,1)=1+(10^(−8))*(8342.12+2406030/(130−1/(lamda^2)) ...
        +(15997/(38.9−1/lamda^2)))*(rho(i,1)/1.221);



    %Calculates index of refraction using Gladstone−Dale for 1 micron
    %wavelength and the density of the flowfield
    ngd(i,1)=1+kgd*rho(i,1);
```

69

```matlab
    end

%Clean Up
 clear kgd i


%end of Routine
```

Listing C.5. datamesh.m

```matlab
%————————————datamesh.m————————————————%
%Routine that takes flow data and puts the data into a grid for iterating
%Created by James C Bowers  Date: 5 Jan 2010
%—————————————variables—————————————————%
%Input Variables
%x= xdata (called in)
%y= y data (called in)
%press = pressure data (called in)
%temp = temperature data (called in)
%rho = density data (called in)
%ned = index of refraction using edlen  (called in)
%ngd = index of refraction using Gladstone−Dale(density)  (called in)
%xx = number of grid points in x direction (first specified)
%yy = number of grid points in y direction (first specified)
%
%Output Variables
%xmid = grid midpoint in x direction
%ymid = grid midpoint in y direction
%xmat= x point array
%ymat = y point array
%tempgrd = Temperature Grid
%pressgrd = Pressure Grid
%rhogrd = Density Grid
%xgrd = X Grid
%ygrd = Y Grid
%nedgrd = Grids the refractive index from edlen
%nedgrd = Grids the refractive index from G−D
%———————————————————————————————————————%

%Pre−Clean Up
 clear xx yy xmid ymid xmat ymat tempgrd pressgrd rhogrd xgrd ygrd nptgrd ngdgrd

%Dimension Setup
xx=1001;
yy=1001;

%Grid Midpoints
xmid=ceil(xx/2);
```

```matlab
ymid=ceil(yy/2);

%Below is Location allocation for gridding the data. This will eventually
%change with the next iteration be conditional upon either data a/o path
xmat=linspace(0,1,xx);  %X Location Allocation
ymat=linspace(0.5,-0.5,yy)';  %Y Location Allocation

%Setting up Grids for current data
tempgrd=griddata(x,y,temp,xmat,ymat);  %Temperature Grid
pressgrd=griddata(x,y,press,xmat,ymat);  %Pressure Grid
rhogrd=griddata(x,y,rho,xmat,ymat);  %Density Grid
xgrd=griddata(x,y,x,xmat,ymat);  %X Grid
ygrd=griddata(x,y,y,xmat,ymat);  %Y Grid
nedgrd=griddata(x,y,ned,xmat,ymat);  %Grids the refractive index from Edlen
ngdgrd=griddata(x,y,ngd,xmat,ymat);  %Grids the refractive index from G-D

%End of Routine
```

Listing C.6. radmesh.m

```
%———————————————radmesh.m—————————————————————————%
%Routine that creates radius spread from x & y points in gridded format
%Created by James C Bowers   Date: 5 Jan 2010
%———————————————————variables—————————————————————————%
%Input Variables
%xgrd = X Grid   (called in)
%ygrd = Y Grid   (called in)
%Output Variables
%ngrd = Grids the radius from x & y grids
%——————————————————————————————————————————————————%


clear rgrd i j


rgrd=zeros(xx,yy); %Initializing radius array


for i=1:xx
    for j=1:yy

        %cleans up the left hand column of x points
        if i==1
            xgrd(j,1)=0;
        end

        %Calculates radius from central point in flow field for structure
        %function calculations
        rgrd(i,j)=sqrt(((xgrd(i,j)-xgrd(xmid,ymid))^2)+((ygrd(i,j)-ygrd(xmid,ymid))^2));

    end
end


clear i j


%end of routine
```

Listing C.7. oplcalc.m

```matlab
%————————————————oplcalc.m————————————————————%
%Routine that calculates optical path length
%Created by James C Bowers   Date: 5 Jan 2010
%————————————————variables————————————————————%
%Input Variables
%nedgrd = Grids the refractive index from edlen  (called in)
%ngdgrd = Grids the refractive index from G−D  (called in)
%dy = y gridspacing (first specified)
%suminted = integration sum for edlen
%sumintgd = integration sum for gladstone−dale
%xx,yy = grid dimensions
%Output variables
%oplgdmean = optical path length mean for row using gladstone−dale
%opledmean = optical path length mean for row using edlen
%opled = optical path length integrated up the column using edlen
%oplgd = optical path length integrated up the column using glad−dale
%————————————————————————————————————————————%


%Pre−Clean up
clear dy suminted sumintgd opled oplgd oplgdmean opledmean i j


dy=0.001;  %Delta y − used for intergration − comes from length and spacing


%Initializing integration sum
suminted=0;
sumintgd=0;


%initializing Matricies
opled=zeros(yy,xx);
oplgd=zeros(yy,xx);
oplgdmean=zeros(yy,1);
opledmean=zeros(yy,1);


for j=1:xx  %Steps through columns for x direction

    for i=yy:−1:1  %Starts at bottom row of column and works up

        %Integrates up column
```

74

```matlab
            suminted=suminted+nedgrd(i,j)*dy;
            sumintgd=sumintgd+ngdgrd(i,j)*dy;

            %Stores OPL at those points
            opled(i,j)=suminted;
            oplgd(i,j)=sumintgd;

        end

        %Resets sumints
        suminted=0;
        sumintgd=0;

    end

    %Calculates the mean of the OPL's as it rises from the bottom by row
    for i=yy:-1:1

        opledmean(i,1)=mean(opled(i,:));
        oplgdmean(i,1)=mean(oplgd(i,:));

    end

    %Post Clean Up
    clear suminted sumintgd i j
```

Listing C.8. opdcalc.m

```
%——————————————————opdcalc.m——————————————————————%
%Routine that calculates optical path difference
%Created by James C Bowers   Date: 5 Jan 2010
%———————————————————variables———————————————————————%
%Input variables
%xx,yy = grid dimensions
%oplgdmean = optical path length mean for row using gladstone-dale
%opledmean = optical path length mean for row using edlen
%opled = optical path length integrated up the column using edlen
%oplgd = optical path length integrated up the column using G-D
%Output Variables
%opded = optical path difference using press-temp
%opdgd = optical path difference using press-temp
%———————————————————————————————————————————————————%
clear i j opded opdgd


opded=zeros(yy,xx);
opdgd=zeros(yy,xx);


for j=1:xx

    for i=yy:-1:1

        opded(i,j)=opled(i,j)-opledmean(i,1);
        opdgd(i,j)=oplgd(i,j)-oplgdmean(i,1);

    end

end


clear i j
```

76

Listing C.9. phaseamp.m

```matlab
%————————————————————phaseamp.m————————————————————————————————%
%Routine that calculates the phase from opd and amplitude of the beam for
%use in subsequent metric calculations.
%Created by James C Bowers   Date: 5 Jan 2010
%——————————————————————————variables————————————————————————————————————%
%Input variables
%xx,yy = grid dimensions
%opdgd = optical path difference using gladstone-dale (called-in)
%opded = optical path difference using edlen (called-in)
%wo = beam waist radius provided (first specified)
%lamda = beam wavelength (called in)
%Output Variables
%thetaed = beam phase at points using edlen
%thetagd = beam phase at points using G-D
%a = beam amplitude at points (assumes normalized peak of 1 at center)
%————————————————————————————————————————————————————————————————————————%


clear wo thetapt thetagd i j a


%Specifies a beam waist radius
wo=0.5;


%Initializing Output matricies for speed
thetaed=zeros(xx,yy);
thetagd=zeros(xx,yy);
a=zeros(xx,yy);


%Phase and Amplitude Calculation Iteration
for i=1:xx
    for j=1:yy


        %Phase at points using OPD & wavelength
        thetaed(i,j)=((-2*pi)/(lamda*10^-6))*opded(i,j);
        thetagd(i,j)=((-2*pi)/(lamda*10^-6))*opdgd(i,j);


        %Natural Log of amplitude assuming Gaussian beam
        a(i,j)=-((xgrd(i,j)-xgrd(xmid,ymid))^2)/(wo^2);
```

```matlab
        end
    end

    %Post Clean Up
    clear i j

    %End of Routine
```

Listing C.10. structure.m

```
%————————————————————structure.m————————————————————————————%
%Routine that calculates the structure functions and then determinens the
%Cn^2's from various methods
%Created by James C Bowers  Date: 5 Jan 2010
%————————————————————————variables——————————————————————————%
%% Input Variables
%dr = radial step size (first specified)
%tol= radius incorporation tolerance for data points (first specified)
%nedgrd = Grids the refractive index from Edlen  (called in)
%ngdgrd = Grids the refractive index from G–D  (called in)
%xx,yy = grid dimensions
%xmid,ymid = grid midpoints
%rgrd = flow radius from center point (called in)
%tempgrd = temperature data from flow (called in)
%thetapt = beam phase at points using press−temp (called in)
%thetagd = beam phase at points using press−temp (called in)
%a = beam amplitude at points (assumes normalized peak of 1 at center)
%% Output variables
%nmax = calculated max number of radial steps
%dngdsum = sum of index difference for average from G–D
%dnedsum = sum of index difference for average from Edlen
%dthetaedsum = sum of phase difference for average from Edlen
%dthetagdsum = sum of phase difference for average from G–D
%dasum = sum of amplitude difference for average
%dtsum = sum of temperature difference for average
%k = number of data points at radius used for average
%pntcnt = collected number of data points for all radii
%r = radius values
%dned = Structure function edlen
%dngd = Structure Function G–D
%cn2ed = Cn2 calculated from edlen
%cn2gd = Cn2 calculated from G–D
%dthetaed = Structure Function for phase for Edlen
%dthetagd = Structure Function for phase for G–D
%da = Structure Function for ln(amplitude)
%dtaed = Combined Struct Function for Amp & Phase for Edlen
%dtagd = Combined Struct Function for Amp & Phase for G–D
%dt = Struct Function for Temperature
```

79

```matlab
%ct2 = Ct2
%cn2t = Cn2 calculated from Ct2
%roed = fried coherance length from Edlen
%rogd = fried coherance length from G-D
%——————————————————————————————————————————————%
%% Pre Clean
clear nmax dr tol nmax dngdsum dnedsum dasum dtsum k i j n
clear pntcnt r dned dngd cn2ed cn2gd dthatapt dtheatgd
clear da dtaed dtagd dt ct2 cn2t roed rogd

nmax=floor(xx/2); %Limits the number of radial steps out from the center
dr=0.001;  %Radial step size

% Because grid is cartesian and the calculations are based on polar
% coordinates I specify a radius tolerance to smooth out the number of
% sample points within my radial grid
tol=0.0005;

% Initializing sums and counters prior to iteration
dnedsum=0;
dngdsum=0;
dthetaedsum=0;
dthetagdsum=0;
dasum=0;
dtsum=0;
k=0;  %Sample point counter
r=zeros(1,nmax);
dned=zeros(1,nmax);
dngd=zeros(1,nmax);
cn2ed=zeros(1,nmax);
cn2gd=zeros(1,nmax);
dthetaed=zeros(1,nmax);
dthetagd=zeros(1,nmax);
da=zeros(1,nmax);
dtaed=zeros(1,nmax);
dtagd=zeros(1,nmax);
dt=zeros(1,nmax);
ct2=zeros(1,nmax);
cn2t=zeros(1,nmax);
roed=zeros(1,nmax);
```

```matlab
rogd=zeros(1,nmax);
ptcnt=zeros(1,nmax);


for n=1:nmax %Radial outward step

    r(n)=n*dr; %Stores current radius

    for i=1:xx
        for j=1:yy

            %Steps through the radius grid to see if the radius point data
            %is with in the step size specified radius +/- the tolerance.
            %If radius meets those criteria it uses the data point to
            %calculate the structure functions
            if rgrd(i,j)≤r(n)+tol && rgrd(i,j)≥r(n)-tol

                %Refractive Index Structure Function
                dnedsum=dnedsum+(abs((nedgrd(i,j)-nedgrd(xmid,ymid)))^2);
                dngdsum=dngdsum+(abs((ngdgrd(i,j)-ngdgrd(xmid,ymid)))^2);

                %Temperature Structure Function
                dtsum=dtsum+(abs((tempgrd(i,j)-tempgrd(xmid,ymid)))^2);

                %Phase Structure Function
                dthetaedsum=dthetaedsum+(abs((thetaed(i,j)-thetaed(xmid,ymid))^2));
                dthetagdsum=dthetagdsum+(abs((thetagd(i,j)-thetagd(xmid,ymid))^2));

                %Amplitude Structure Function
                dasum=dasum+abs((a(i,j)-a(xmid,ymid))^2);


                k=k+1;  %Sample Count Number for averaging

            end

        end
    end

    %Average of Dn for the specified radius
    dned(n)=dnedsum/k;
    dngd(n)=dngdsum/k;
```

```matlab
%Calculates Cn^2 from Refractive Index Struture function assuming r^(2/3)
cn2ed(n)=(dned(n)/((r(n))^(2/3)));
cn2gd(n)=(dngd(n)/((r(n))^(2/3)));


%Calculates Cn^2 from Temperature Struture function assuming r^(2/3)
dt(n)=dtsum/k;
ct2(n)=(dt(n)/((r(n))^(2/3)));
cn2t(n)=(ct2(n))*((79*10^(-6))*1001.3/(288.15^2))^2;


%Structure function for Phase
dthetaed(n)=dthetaedsum/k;
dthetagd(n)=dthetagdsum/k;


%Structure function for Amplitude
da(n)=dasum/k;


%Combined Structure Function
dtaed(n)=da(n)+dthetaed(n);
dtagd(n)=da(n)+dthetagd(n);


%Fried Coherance length calculation
roed(n)=r(n)/((dtaed(n)/6.88)^(3/5));
rogd(n)=r(n)/((dtagd(n)/6.88)^(3/5));


%Calculates Cn^2 from fried parameter
cn2roed(n)=((0.185)*(((lamda*10^(-6))^(6/5))/((1^(3/5))*(roed(n)))))^(5/3);
cn2rogd(n)=((0.185)*(((lamda*10^(-6))^(6/5))/((1^(3/5))*(rogd(n)))))^(5/3);


%Calculates ro from Cn^2
rocn2ed(n)=0.185*(((lamda*10^(-6))^(6/5))/((1^(3/5))*(cn2ed(n)^(3/5))));
rocn2gd(n)=0.185*(((lamda*10^(-6))^(6/5))/((1^(3/5))*(cn2gd(n)^(3/5))));


%Calculates Phase Structure function from Cn^2
dthetacn2ed(n)=2.91*(((2*pi)/(lamda*10^(-6)))^(2))*(r(n)^(5/3))*cn2ed(n);
dthetacn2gd(n)=2.91*(((2*pi)/(lamda*10^(-6)))^(2))*(r(n)^(5/3))*cn2gd(n);


%Stores the number of sample points for pure statistical info
ptcnt(n)=k;
```

```matlab
        %Resets all counters/sums for the next iteration
        dnedsum=0;
        dngdsum=0;
        dthetaedsum=0;
        dthetagdsum=0;
        dasum=0;
        k=0;

end

%% Post Clean
clear i j k dasum dthetagdsum dthetaedsum dngdsum dnedsum
```

Listing C.11. flowviz.m

```matlab
%———————————————flowviz.m———————————————————————%
%Routine that takes flow data and plots it for visualization
%Created by James C Bowers   Date: 5 Jan 2010
%————————————————variables—————————————————————%
%Input Variables
%tempgrd = Temperature Grid  (called in)
%pressgrd = Pressure Grid  (called in)
%rhogrd = Density Grid  (called in)
%xgrd = X Grid  (called in)
%ygrd = Y Grid  (called in)
%nedgrd = Grids the refractive index from Edlen  (called in)
%ngdgrd = Grids the refractive index from G-D  (called in)
%figcnt = figure counter  (first specified)
%———————————————————————————————————————————————%


clear figcnt

figcnt=1;

figure(figcnt)
subplot(1,3,1),mesh(xgrd,ygrd,tempgrd)
axis([0 1 -0.5 0.5])
title('Temperture of Flow Field (K)')
xlabel('X')
ylabel('Y')
zlabel('Temperature(K)')
subplot(1,3,2),mesh(xgrd,ygrd,rhogrd)
axis([0 1 -0.5 0.5])
title('Density of Flow Field (kg/m^3)')
xlabel('X')
ylabel('Y')
zlabel('Density (kg/m^3)')
subplot(1,3,3),mesh(xgrd,ygrd,pressgrd)
axis([0 1 -0.5 0.5])
title('Pressure of Flow Field (mbars)')
xlabel('X')
ylabel('Y')
zlabel('Pressure (mbars)')
```

```matlab
figcnt=figcnt+1;

figure(figcnt)
subplot(2,2,1),mesh(xgrd,ygrd,nedgrd)
axis([0 1 -0.5 0.5])
title('Refractive Index(Edlen) of Flow Field')
xlabel('X')
ylabel('Y')
zlabel('n')
subplot(2,2,2),mesh(xgrd,ygrd,ngdgrd)
axis([0 1 -0.5 0.5])
title('Refractive Index(Gladstone Dale) of Flow Field')
xlabel('X')
ylabel('Y')
zlabel('n')
subplot(2,2,3),mesh(xgrd,ygrd,opdgd)
axis([0 1 -0.5 0.5])
title('Optical Path Difference (Gladstone Dale) of Flow Field')
xlabel('X')
ylabel('Y')
zlabel('OPD')
subplot(2,2,4),mesh(xgrd,ygrd,opded)
axis([0 1 -0.5 0.5])
title('Optical Path Difference (Edlen) of Flow Field')
xlabel('X')
ylabel('Y')
zlabel('OPD')

figcnt=figcnt+1; %updates figure counter

%end of subroutine
```

Listing C.12. metric.m

```
%————————————————metric.m————————————————————————%
%Routine that takes the import optics data calculated and plots or presents
%that data in a visual format
%Created by James C Bowers  Date: 5 Jan 2010
%————————————————————variables————————————————————————%
%% Input Variables
%figcnt = figure counter (called in)
%opded = optical path difference using edlen (called in)
%opdgd = optical path difference using G-D (called in)
%xmat = linear x location matrix (called in)
%r = radii for basis of structure funtion from center (called in)
%dned = Structure function from edlen (called in)
%dngd = Structure function from G-D (called in)
%cn2gd = Cn^2 from G-D (called in)
%cn2edlen = Cn^2 from edlen (called in)
%cn2t = Cn^2 from Temperature Cn^2 (called in)
%roed = fried coherence length using edlen (called in)
%rogd = fried coherence length using G-D (called in)
%% Output Variables
%diff = absolute difference between opd's
%————————————————————————————————————————————————%


%% Comparison Plot
%Plots the OPD's for the top row of the gridpoints


diff(1,:)=abs(opded(1,:)-opdgd(1,:));


figure(figcnt)
subplot(2,1,1),plot(xmat,opded(1,:),xmat,opdgd(1,:))
title('Optical Path Difference Along Streamwise Direction Comparison')
xlabel('X(m)')
ylabel('OPD')
legend('Edlen','Gladstone-Dale','location','bestoutside')
subplot(2,1,2),plot(xmat,diff,'r')
title('Optical Path Difference Comparison Absolute Difference')
xlabel('X(m)')
ylabel('Absolute Difference')
```

86

```matlab
figcnt=figcnt+1;

%% Data Visualization

figure(figcnt)
loglog(r,dned,'o',r,dngd,'xk')
title('Calculated Structure Function with r')
xlabel('r (m)')
ylabel('Dn')
legend('Edlen','Gladstone-Dale','Location','Bestoutside')

figcnt=figcnt+1;

figure(figcnt)
loglog(r,cn2ed,'og',r,cn2gd,'xk',r,cn2t,'+r',r,cn2roed,'*m',r,cn2rogd,'.b')
title('Calculated Cn^2 with r^2^/^3')
xlabel('r (m)')
ylabel('Cn^2')
legend('Edlen','G-D','CT^2','r_o (Edlen)','r_o (G-D)','Location','Bestoutside')

figcnt=figcnt+1;

figure(figcnt)
loglog(r,roed,'o',r,rogd,'xk',r,rocn2ed,'*m',r,rocn2gd,'.b')
title('Calculated r_o')
xlabel('r (m)')
ylabel('r_o (m)')
legend('Edlen','Gladstone-Dale','Cn^2 (Edlen)','Cn^2 (G-D)','Location','Bestoutside')

figcnt=figcnt+1;

figure(figcnt)
loglog(r,dthetaed,'o',r,dthetagd,'xk',r,dthetacn2ed,'*m',r,dthetacn2gd,'.b')
title('Structure Function of Phase comparison')
xlabel('r (m)')
ylabel('Dtheta')
legend('Edlen','Gladstone-Dale','Cn^2 (Edlen)','Cn^2 (G-D)','Location','Bestoutside')

%End of Routine
```

Bibliography

[1] Aguirre, Roberto C., Haris J. Catrakis, and H. Atassi. "Aero-Optical Wavefronts and Scale-Local Characterization in Large Reynolds Number Compressible Turbulence". *AIAA Journal*, 42(10):1982–1990, 2004.

[2] Andrews, Larry C. and Ronald L. Phillips. *Laser Beam Propagation through Random Media*. SPIE, Bellingham, WA, Second edition, 2005.

[3] Catrakis, Haris J., Philip J. Garcia, and Jennifer C. Nathman. "Cumulative Aero-Optical Interactions Along Laser Beam Propagation Paths: Experiments and Computations". *44th AIAA Aerospace Sciences Meeting and Exhibit, 9-12 January 2006, Reno, NV*. AIAA 2006-1495, AIAA, 2006.

[4] Clark, Timothy T. "Introduction to Turbulence Theory and Modeling for Optical Applications". *9th Annual Directed Energy Symposium*. DEPS, DEPS, 2006.

[5] Fried, D. L. "Optical herodyne Dectection of an Atmospherically distorted Signal Wave Front". *Proceedings of the IEEE*, 55:57–67, 1967.

[6] Golbraikh, E. and N. S. Kopeika. "Turbulence strength parameter in laboratory and natural optical experiments in non-Kolmogorov cases". *Optics Communications*, 44(4):333–338, 2004.

[7] Grismer, M. J., W. Z. Strang, R. F. Tomaro, and F. C. Witzeman. "Cobalt: A Parallel, Implicit, Unstructured Euler/Navier-Stokes Flow Solver". *Advances in Engineering Software*, 29:365–373, 1998.

[8] Ishimaru, Akira. *Wave Propagation and Scattering in Random Media*. IEEE Press, New York, NY, First edition, 1978.

[9] Kolmogorov, A. N. "The Local Structure of Turbulence in Incompressible Viscous fluid for very large Reynold's Numbers". *Royal Society (London), Proceedings, Series A - Mathematical and Physical Sciences*, 434(1890):9–13, 1991.

[10] Monin, A. S. and A. M. Yaglom. *Statistical Fluid Mechanics: Mechanics of Turbulence*. MIT Press, Cambridge, MA, First edition, 1965.

[11] Perram, Glen P., Salvatore J. Cusumano, Robert L. Hengehold, and Steven T. Fiorino. *An Introduction to Laser Weapon Systems*. Directed Energy Professional Society, Albuquerque, NM, First edition, 2010.

[12] Rennie, M., Z. Ponder, S. Gordeyev, A. Nightingale, and E. Jumper. "Numerical Investigation of Two-Dimensional Compressible Shear layer and Comparison to Weakly Compressible Model". *DEPS March 2008*. 2008.

[13] Shugaev, Fedor V., Evgeni N. Terentiev, Ludmila S. Shtemenko, Olga I. Dokukina, and Oksana A. Ignateva. "Characterization of a Laser Beam in Turbulent Atmosphere". *Proceedings of SPIE*, 5981:127–138, 2005.

[14] Siegenthaler, John P., Eric J. Jumper, and Stanislav Gordeyev. "Atmospheric Propagation Vs. Aero-Optics". *46th AIAA Aerospace Sciences Meeting and Exhibit, 7-10 January 2008, Reno, NV*. AIAA 2008-1076, AIAA, 2008.

[15] Sirazetdinov, Vladamir S. and Inga V. Ivanova. "Simulation of laser beam propagation through turubulent medium by means of Fresnel transformation". *Proceedings of SPIE*, 5743:81–93, 2004.

[16] Strang, W. Z., R. F. Tomaro, and M. J. Grismer. "The Defining Methods of Cobalt60: A Parallel, Implicit, Unstructured Euler/Navier-Stokes Flow Solver". *37th AIAA Aerospace Sciences Meeting and Exhibit, January 1999, Reno, NV*. AIAA 99-0786, AIAA, 1999.

[17] Tennekes, H. and J. L. Lumley. *A First Course in Turbulence*. MIT Press, Cambridge, MA, First edition, 1972.

[18] Toselli, Italo, Larry C. Andrews, Ronald L Phillips, and Valter Ferrero. "Free-space optical system performance for laser beam propagation through non-Kolmogorov turbulence". *Optical Engineering: The Journal of the Society of Photo-Optical Instrumentation Engineers*, 47(2):26003–1–26003–9, 2008.

[19] Visbal, Miguel. "Numerical Simulation of Aero-Optical Aberration Through Weakly-Compressible Shear Layers". *39th AIAA Fluid Dynamics Conference, 22-25 June 2009, San Antonio, TX*. AIAA 2009-4298, AIAA, 2009.

[20] Wallace, John M. and Peter V. Hobbs. *Atmospheric Science: An Introductory Survey*. Elsevier, Oxford, UK, Second edition, 2006.

[21] Wolfe, William L. and George John Zissis. *The Infrared Handbook*. Office of Naval Research, Dept. of the Navy, Washington, D.C., Second edition, 1978.

[22] Zubair, Fazlul R. and Haris J. Catrakis. "Aero-Optical Resolution Robustness in Tubulent Seperated Shear Layers at Large Reynolds Numbers". *AIAA Journal*, 45(11):2721–2728, 2007.

Vita

Capt James Bowers was born in Greensboro, North Carolina. After graduating as his class valedictorian of Eastern Guilford High School in 1999, he studied Aerospace Engineering at North Carolina State University (NCSU). He graduated from NCSU with a Bachelor's of Science degree in Aerospace Engineering in May of 2004. Capt Bowers received his commission into the United States Air Force in May of 2004, through successful completion of the Reserve Officer Training Corps program while at NCSU. Following graduation, he was assigned to the Air Force Research Laboratory Air Vehicles Directorate (AFRL/RB). He spent his first two years with AFRL/RB in the Computational Sciences Branch using Computational Fluid Dynamics (CFD) tools to provide test support for wind tunnel experiments. He then transferred into the Aerodynamic Configuration Branch where he served as a program manager for Aero-Structural Efficiency technology. His last year with AFRL/RB was spent as Directorate Executive Officer. Following his assignment with AFRL/RB, he started graduated school at the Air Force Institute of Technology (AFIT) in May of 2008 and he is currently completing his Master's degree in Applied Physics. His follow-on assignment is to the 453rd Electronic Warfare Squadron (453 EWS) at Lackland AFB, Texas.

REPORT DOCUMENTATION PAGE

Form Approved
OMB No. 074-0188

1. REPORT DATE	2. REPORT TYPE	3. DATES COVERED *(From – To)*
25 March 2010	Master's Thesis	Jan 2009 – Mar 2010

4. TITLE AND SUBTITLE	5a. CONTRACT NUMBER
Numerical Investigation of Statistical Turbulence Effects on Beam Propagation through 2-D Shear Mixing Layer	5b. GRANT NUMBER
	5c. PROGRAM ELEMENT NUMBER
6. AUTHOR(S)	5d. PROJECT NUMBER
Bowers, James C., Captain, USAF	5e. TASK NUMBER
	5f. WORK UNIT NUMBER

7. PERFORMING ORGANIZATION NAMES(S) AND ADDRESS(S)	8. PERFORMING ORGANIZATION REPORT NUMBER
Air Force Institute of Technology Graduate School of Engineering and Management (AFIT/ENY) 2950 Hobson Way, Building 640 WPAFB OH 45433-8865	AFIT/GAP/ENP/10-M03

9. SPONSORING/MONITORING AGENCY NAME(S) AND ADDRESS(ES)	10. SPONSOR/MONITOR'S ACRONYM(S) HEL-JTO
High Energy Laser-Joint Technology Office (HEL-JTO) 901 University Blvd SE Albuquerque, NM 87106	11. SPONSOR/MONITOR'S REPORT NUMBER(S)

12. DISTRIBUTION/AVAILABILITY STATEMENT

APPROVED FOR PUBLIC RELEASE; DISTRIBUTION UNLIMITED.

13. SUPPLEMENTARY NOTES

14. ABSTRACT
A methodology is developed for determining the validity of making a statistical turbulent approach using Kolmogorov theory to an aero-optical turbulent flow. Kolmogorov theory provides a stochastic method that has a greatly simplified and robust method for calculating atmospheric turbulence effects on optical beam propagation, which could simplify similar approaches to chaotic aero-optical flows. A 2-D laminar Navier-Stokes CFD Solver (AVUS) is run over a splitter plate type geometry to create an aero-optical like shear mixing layer turbulence field. A Matlab algorithm is developed to import the flow data and calculates the structure functions, structure constant, and Fried Parameter (r_o) and compares them to expected Kolmogorov distributions assuming an $r^{2/3}$ power law. The range of C_n^2's developed from the structure functions are not constant with separation distance, and ranged between 10^{-12}-10^{-10}. There is a consistent range of data overlap within the C_n^2's derived from various methods for separation distances within the range 0.01m-0.02m. Within this range r_o is found to be approximately 0.05m which is a reasonable value. This particular 2-D shear mixing layer was found to be non-Kolmogorov, but further grid refinement and data sampling may provide a more Kolmogorov like distribution.

15. SUBJECT TERMS
Optical beam propagation; atmospheric turbulence; aero-optics; Kolmogorov Theory; modeling & simulation

16. SECURITY CLASSIFICATION OF:			17. LIMITATION OF ABSTRACT	18. NUMBER OF PAGES	19a. NAME OF RESPONSIBLE PERSON
a. REPORT	b. ABSTRACT	c. THIS PAGE	UU		Dr. Steven T. Fiorino, AFIT/ENP
U	U	U		105	19b. TELEPHONE NUMBER *(Include area code)* (937) 255-3636 ext 4506

Standard Form 298 (Rev. 8-98)
Prescribed by ANSI Std. Z39-18